

The First Galaxies: Assembly, Cooling and the Onset of Turbulence

Thomas H. Greif^{1,2,3*}, Jarrett L. Johnson², Ralf S. Klessen¹ and Volker Bromm²

¹ *Institut für theoretische Astrophysik, Albert-Ueberle Strasse 2, 69120 Heidelberg, Germany*

² *Department of Astronomy, University of Texas, Austin, TX 78712, USA*

³ *Fellow of the International Max Planck Research School for Astronomy and Cosmic Physics at the University of Heidelberg*

20 February 2019

ABSTRACT

We investigate the properties of the first galaxies at $z \gtrsim 10$ with highly resolved numerical simulations, starting from cosmological initial conditions and taking into account all relevant primordial chemistry and cooling. A first galaxy is characterized by the onset of atomic hydrogen cooling, once the virial temperature exceeds $\simeq 10^4$ K, and its ability to retain photoheated gas. We follow the complex accretion and star formation history of a $\simeq 5 \times 10^7 M_\odot$ system by means of a detailed merger tree and derive an upper limit on the number of Population III stars formed prior to its assembly. We investigate the thermal and chemical evolution of infalling gas and find that partial ionization at temperatures $\gtrsim 10^4$ K catalyzes the formation of H_2 and HD, allowing the gas to cool to the temperature of the CMB. Depending on the strength of radiative and chemical feedback, primordial star formation might be dominated by intermediate-mass Pop III stars formed during the assembly of the first galaxies. Accretion onto the nascent galaxy begins with hot accretion, where gas is accreted directly from the IGM and shock-heated to the virial temperature, but is quickly accompanied by a phase of cold accretion, where the gas cools in filaments before flowing into the parent halo with high velocities. The latter drives supersonic turbulence at the center of the galaxy and could lead to very efficient chemical mixing. The onset of turbulence in the first galaxies thus likely marks the transition to Pop II star formation.

Key words: stars: early-type – stars: formation – galaxies: formation – galaxies: high-redshift – cosmology: theory – early Universe.

1 INTRODUCTION

Understanding the formation of the first stars and galaxies at the end of the cosmic dark ages is one of the most important challenges in modern cosmology (Barkana & Loeb 2001; Bromm & Larson 2004; Ciardi & Ferrara 2005; Glover 2005). In the standard Λ CDM cosmology, the first stars, termed Population III (Pop III), are predicted to have formed in dark matter (DM) ‘minihaloes’ with virial mass $\sim 10^6 M_\odot$ at $z \sim 20$ (Bromm et al. 1999, 2002; Nakamura & Umemura 2001; Abel et al. 2000, 2002; Yoshida et al. 2003, 2006; Gao et al. 2007; O’Shea & Norman 2007). Based on molecular hydrogen cooling, the gas can cool to $\simeq 200$ K and becomes Jeans-unstable once the central clump attains $\simeq 10^3 M_\odot$. Such high temperatures lead to efficient accretion onto the protostellar core and imply that the first stars were predom-

inantly very massive, with $M_* \gtrsim 100 M_\odot$ (Omukai & Palla 2003; Bromm & Loeb 2004; O’Shea & Norman 2007; but see Tan & McKee 2004; Ripamonti 2007; McKee & Tan 2007; McGreer & Bryan 2008).

Due to their primordial composition, massive Pop III stars have smaller radii than their present-day counterparts and their surface temperatures can exceed $\simeq 10^5$ K, resulting in high photon yields (Tumlinson & Shull 2000; Bromm et al. 2001; Schaerer 2002; Tumlinson et al. 2003). Consequently, they exert strong feedback on the intergalactic medium (IGM) via radiation in the Lyman-Werner (LW) bands, which readily destroys molecular hydrogen (Glover & Brand 2001; Machacek et al. 2001; Ricotti et al. 2001; Omukai & Yoshii 2003; Greif & Bromm 2006; Mesinger et al. 2006; O’Shea & Norman 2008; Johnson et al. 2007b; Wise & Abel 2007d), and ionizing radiation giving rise to the first H II regions (Kitayama et al. 2004; Whalen et al. 2004; Alvarez et al. 2006; Susa & Umemura 2006; Yoshida et al. 2007;

* E-mail: tgreif@ita.uni-heidelberg.de

Ahn & Shapiro 2007; Abel et al. 2007; Johnson et al. 2007a; Whalen et al. 2007). Furthermore, a yet unknown fraction of massive, metal-free stars is expected to end in extremely violent supernova (SN) explosions (Heger & Woosley 2002; Heger et al. 2003), profoundly affecting the IGM in terms of dynamics and chemical enrichment (Bromm et al. 2003; Mackey et al. 2003; Norman et al. 2004; Salvaterra et al. 2004; Yoshida et al. 2004; Kitayama & Yoshida 2005; Machida et al. 2005; Greif et al. 2007; Whalen et al. 2008). Since primordial star formation initially occurs in mini-haloes that constitute the progenitors of the first galaxies, stellar feedback is expected to play an important role during their assembly.

When and where did the first galaxies form? According to the bottom-up character of structure formation, as described by standard Press-Schechter theory (Press & Schechter 1974), the first $\gtrsim 5 \times 10^7 M_\odot$ haloes assembled at $z \gtrsim 10$ via hierarchical merging. This mass scale is set by the onset of atomic hydrogen cooling once the virial temperature exceeds $\simeq 10^4$ K; these objects have therefore frequently been termed ‘atomic cooling haloes’. Henceforth, we will synonymously use the term ‘first galaxy’, as these haloes can retain photoheated gas and therefore might, for the first time, maintain self-regulated star formation in a multi-phase, interstellar medium (Thoul & Weinberg 1996; Mac Low & Ferrara 1999; Madau et al. 2001; Mori et al. 2002; Oh & Haiman 2002; Ricotti et al. 2002a,b; Scannapieco et al. 2002; Thacker et al. 2002; Wada & Venkatesan 2003; Dijkstra et al. 2004; Read et al. 2006; Ricotti et al. 2008).

What types of stars are expected to form during the assembly of the first galaxies? Depending on the primordial initial mass function (IMF) and the strength of radiative and SN-driven feedback, the IGM could be heavily enriched with metals prior to the onset of second-generation star formation (Bromm et al. 2003; Greif et al. 2007; Wise & Abel 2007c). The existence and precise value of a critical metallicity for the transition to Pop II is still vigorously debated, and has originally been discussed in the context of fine-structure versus dust cooling (Bromm & Loeb 2003b; Schneider et al. 2003; Frebel et al. 2007; Jappsen et al. 2007; Smith & Sigurdsson 2007). In the former case, critical metallicities of $Z_{\text{crit}} \simeq 10^{-3.5} Z_\odot$ have been found (Bromm et al. 2001; Santoro & Shull 2006), while in the latter case uncertainties in the dust composition and gas-phase depletion lead to a range of possible values, $10^{-6} \lesssim Z_{\text{crit}} \lesssim 10^{-5} Z_\odot$ (Omukai et al. 2005; Schneider et al. 2006; Tsuribe & Omukai 2006). Somewhat transcending this debate, recent simulations have shown that a single SN explosion might enrich the local IGM to well above any critical metallicity (Bromm et al. 2003; Greif et al. 2007; Wise & Abel 2007c), forcing an early transition in star formation mode (Clark et al. 2008). However, if radiative feedback was sufficiently strong, the bulk of primordial star formation might have occurred in systems that cool via atomic hydrogen lines (Greif & Bromm 2006; O’Shea & Norman 2008; Johnson et al. 2007b). In light of these uncertainties, we investigate the formation of a first galaxy in the limiting case of no feedback, allowing us to focus on the chemistry, cooling and development of turbulence during the assembly of the atomic cooling halo.

Theoretical investigations have recently pointed to-

wards the existence of two physically distinct populations of metal-free stars (Uehara & Inutsuka 2000; Mackey et al. 2003; Johnson & Bromm 2006). Gas cooling primarily via molecular hydrogen leads to the formation of $\gtrsim 100 M_\odot$ stars, termed Pop III.1, while in regions of previous ionization hydrogen deuteride (HD) likely enables the formation of $\gtrsim 10 M_\odot$ stars, termed Pop III.2 (Tan & McKee 2007). This latter mode had previously been termed Pop II.5 (Mackey et al. 2003; Greif & Bromm 2006; Johnson & Bromm 2006). Scenarios providing a substantial degree of ionization include relic H II regions (Nagakura & Omukai 2005), dense shells produced by energetic SN explosions (Bromm et al. 2003; Mackey et al. 2003; Salvaterra et al. 2004; Machida et al. 2005), and structure formation shocks in the virialization of the first galaxies (Oh & Haiman 2002; Greif & Bromm 2006). In the former case, numerical simulations have confirmed that the gas can cool to the temperature of the cosmic microwave background (CMB), reducing the Jeans-mass by almost an order of magnitude compared to the truly primordial case (Johnson et al. 2007a; Yoshida et al. 2007), while we here set out to investigate the effects of partial ionization and molecule formation during the assembly of the first galaxies. One of the key questions is therefore whether the gas can cool to the CMB limit and thus enable the formation of Pop III.2 stars.

Another important aspect concerning the baryonic collapse of the first galaxies is the development of turbulence. While turbulence does not seem to play a role in mini-haloes, at least on scales comparable to their virial radius (Yoshida et al. 2006), turbulent motions could become important in more massive haloes, where accretion of cold gas from filaments in combination with a softened equation of state drives strong shocks (Kereš et al. 2005; Wise & Abel 2007b; Sancisi et al. 2008), possibly leading to vigorous fragmentation and the formation of the first star clusters (Clark et al. 2008). This would mark the first step towards conditions similar to present-day star formation, where supersonic turbulent velocity fields determine the fragmentation properties of the gas. In our present study, we investigate the role of turbulence by analysing the velocity field and energy content of the galaxy during virialization. We then discuss the likely fragmentation properties of the gas and the consequences for second-generation star formation.

The final ingredient of early galaxy formation is the co-evolution of massive black holes (MBHs) and the surrounding stellar system, leading in extreme cases to the formation of the highest redshift quasars observed at $z \gtrsim 6$. The most sophisticated simulations of supermassive black hole (SMBH) growth to date have been conducted by Li et al. (2007), but their resolution was insufficient to trace the origin of SMBHs below $\simeq 10^5 M_\odot$. Such SMBHs could form via direct collapse of isothermal gas in atomic cooling haloes in the presence of a strong photo-dissociating background (Bromm & Loeb 2003a; Koushiappas et al. 2004; Begelman et al. 2006; Lodato & Natarajan 2006; Spaans & Silk 2006; Wise et al. 2007), or via merging and accretion of gas onto the compact remnants of Pop III stars (Madau & Rees 2001; Schneider et al. 2002; Islam et al. 2003; Volonteri et al. 2003; Volonteri & Rees 2005; Johnson & Bromm 2007; Pelupessy et al. 2007; Wise et al. 2007). Here, we investigate the fate of BHs seeded by the remnants of Pop III stars and

their prospect of growing into SMBHs at the centers of the first galaxies. Finally, we provide an estimate for the amplitude of ionizing and molecule-dissociating radiation emitted by the accretion disk around the central BH.

The structure of our work is as follows. In Section 2, we discuss the setup of the cosmological simulations, the implementation of multiple levels of refinement and our sink particle algorithm. We then describe the hierarchical assembly of the galaxy (Section 3), its cooling and star formation properties (Section 4), and the development of turbulence (Section 5). In Section 6, we discuss the growth of the BH at the center of the galaxy, and in Section 7 we summarize our results and assess their implications. For consistency, all distances are physical (proper), unless noted otherwise.

2 NUMERICAL METHODOLOGY

To investigate the formation of the first galaxies with adequate accuracy, our simulations must resolve substructure on small scales as well as tidal torques and global gravitational collapse on much larger scales. We capture all the relevant dynamics by performing a preliminary simulation with a coarse base resolution, but refine around the point of highest fluctuation power. This ensures that the region containing the mass of the galaxy is well resolved and that a given number of particles is distributed efficiently.

2.1 Initial Setup

The simulations are carried out in a cosmological box of linear size $\simeq 700$ kpc (comoving), and are initialized at $z = 99$ according to a concordance Λ cold dark matter (Λ CDM) cosmology with matter density $\Omega_m = 1 - \Omega_\Lambda = 0.3$, baryon density $\Omega_b = 0.04$, Hubble parameter $h = H_0 / (100 \text{ km s}^{-1} \text{ Mpc}^{-1}) = 0.7$, spectral index $n_s = 1.0$, and normalization $\sigma_8 = 0.9$ (Spergel et al. 2003). Density and velocity perturbations are imprinted at recombination with a Gaussian distribution, and we apply the Zeldovich approximation to propagate the fluctuations to $z = 99$, when the simulation is started. To capture the chemical evolution of the gas, we follow the abundances of H, H^+ , H^- , H_2 , H_2^+ , He, He^+ , He^{++} , and e^- , as well as the five deuterium species D, D^+ , D^- , HD and HD^- . We include all relevant cooling mechanisms, i.e. H and He atomic line cooling, bremsstrahlung, inverse Compton scattering, and collisional excitation cooling via H_2 and HD (see Johnson & Bromm 2006).

2.2 Refinement and Sink Particle Formation

In a preliminary run with 64^3 particles per species (DM and gas), we locate the formation site of the first $\simeq 5 \times 10^7 M_\odot$ halo. This object is just massive enough to activate atomic hydrogen cooling and fulfil our prescription for a galaxy. We subsequently carry out a standard hierarchical zoom-in procedure to achieve high mass resolution inside the region destined to collapse into the galaxy (e.g. Navarro & White 1994; Tormen et al. 1997; Gao et al. 2005). We apply three consecutive levels of refinement centered on this location, such that a single parent particle is replaced by a maximum

of 512 child particles. The particle mass in the region containing the comoving volume of the galaxy with an extent of $\simeq 200$ kpc (comoving) is $\simeq 100 M_\odot$ in DM and $\simeq 10 M_\odot$ in gas. This allows a baryonic resolution of $\simeq 10^3 M_\odot$, such that the ‘loitering state’ in minihaloes at $T \simeq 200$ K and $n_H \simeq 10^4 \text{ cm}^{-3}$ is marginally resolved (Bromm et al. 2002).

To follow the growth of BHs seeded by the collapse of Pop III.1 stars in minihaloes, we apply a slightly modified version of the sink particle algorithm introduced in Johnson & Bromm (2007). Specifically, we create sink particles once the density exceeds $n_H = 10^4 \text{ cm}^{-3}$ and immediately accrete all particles within the resolution limit of the highest-density particle, resulting in an initial sink particle mass of $\simeq 2 \times 10^3 M_\odot$. Further accretion is governed by the following criteria: particles must be bound ($E_{\text{kin}} < |E_{\text{pot}}|$), have a negative divergence in velocity, and fall below the Bondi radius:

$$r_B = \frac{\mu m_H G M_{\text{BH}}}{k_B T}, \quad (1)$$

where μ is the mean molecular weight, M_{BH} the mass of the black hole, and T the temperature of the gas at the location of the sink particle, determined by a mass-weighted average over all accreted particles. Typical values for the initial Bondi radius are $r_B \simeq 5$ pc. Here, we do not model radiative feedback that would result from accretion, and we therefore overestimate the Bondi radius and consequently the growth of the BH. We further assume that BH mergers occur instantaneously once their separation falls below the resolution limit, provided that their relative velocity is smaller than the escape velocity. Our idealized treatment provides a robust upper limit on the growth rate of BHs during the assembly of the first galaxies, but a more realistic calculation including the effects of feedback will be presented in future work.

3 FIRST GALAXY ASSEMBLY

Among the key questions concerning the formation of the first galaxies are the degree of complexity associated with the halo assembly process, the role of previous star formation in minihaloes, the chemical and thermal evolution of infalling gas, and the development of turbulence. To answer these questions, we first discuss the gravitational evolution of the DM with a merger tree that reconstructs the mass accretion history of the resulting atomic cooling halo, and allows us to determine the maximum amount of previous star formation in its progenitor haloes.

3.1 Atomic Cooling Criterion

Possibly the most important characteristic distinguishing the first galaxies from their lower-mass minihalo predecessors is their ability to cool via atomic hydrogen lines, which softens the equation of state at the virial radius and allows a fraction of the potential energy to be converted into kinetic energy. At high redshift, the virial temperature of a system with virial mass M_{vir} can be expressed as:

$$T_{\text{vir}} \simeq 10^4 \text{ K} \left(\frac{M_{\text{vir}}}{5 \times 10^7 M_\odot} \right)^{2/3} \left(\frac{1+z}{10} \right), \quad (2)$$

such that a $5 \times 10^7 M_\odot$ halo at $z \simeq 10$ is just massive enough to fulfil the atomic cooling criterion (Oh & Haiman 2002). Related to this, they have the ability to retain gas photoheated by hydrogen ionization (Dijkstra et al. 2004), likely allowing self-regulated star formation for the first time. Furthermore, it is often argued that star formation in atomic cooling haloes provided the bulk of the photons for reionization due to efficient shielding from LW radiation (Bromm & Loeb 2003a; Greif & Bromm 2006; Haiman & Bryan 2006; Choudhury et al. 2008; Wise & Abel 2007a). They may have been the key drivers of early IGM enrichment (Madau et al. 2001), and the host systems for the formation of the first low-mass stars that can be probed in the present-day Milky Way via stellar archaeology (Frebel et al. 2007; Karlsson et al. 2007). Their formation thus marks an important milestone in cosmic history, and in light of upcoming observations it is particularly important to understand the properties of these systems.

3.2 Cosmological Abundance

How common are atomic cooling haloes at the redshifts we consider? A frequently used tool to estimate their abundance is the Press-Schechter mass function (Press & Schechter 1974), which provides an analytic expression for the number of DM haloes per mass and comoving volume. Even though the Press-Schechter mass function is inaccurate at low redshifts compared to other analytic estimates such as the Sheth-Tormen mass function (Sheth & Tormen 2002), it provides a good fit to numerical simulations at the early times we are interested in (Jang-Condell & Hernquist 2001; Heitmann et al. 2006; Reed et al. 2007). In Fig. 1, we show the Press-Schechter mass functions for $z \simeq 30$ and 10 (solid and dotted line, respectively), while the symbols indicate the halo distribution extracted from the simulation by the group-finding algorithm HOP (Eisenstein & Hut 1998). The simulation and the analytic estimate generally agree, although there is large scatter due to the finite box size. Better agreement could be expected if one accounted for the fluctuation power on scales greater than the computational box (see Yoshida et al. 2003). At redshift $z \simeq 10$, one expects to find roughly 10 atomic cooling haloes per cubic Mpc (comoving), i.e. of order unity in our computational box of length $\simeq 700$ kpc (comoving). Indeed, in our simulation a single $5 \times 10^7 M_\odot$ halo forms by $z \simeq 10$.

3.3 Assembly of Atomic Cooling Halo

In the Λ CDM paradigm, structure formation proceeds hierarchically, with small objects collapsing first and subsequently growing via merging. This behaviour eventually leads to the formation of haloes massive enough to fulfil the atomic cooling criterion. In Fig. 2, we show the DM overdensity, gas density and temperature averaged along the line of sight at three different output times. The brightest regions in the DM distribution mark haloes in virial equilibrium, according to the commonly used criterion $\rho/\bar{\rho} \simeq 178$, where ρ and $\bar{\rho}$ denote the local and background density. White crosses denote the formation sites of Pop III.1 stars in minihaloes. The first star-forming minihalo at the center of the box assembles at $z \simeq 23$ and subsequently grows

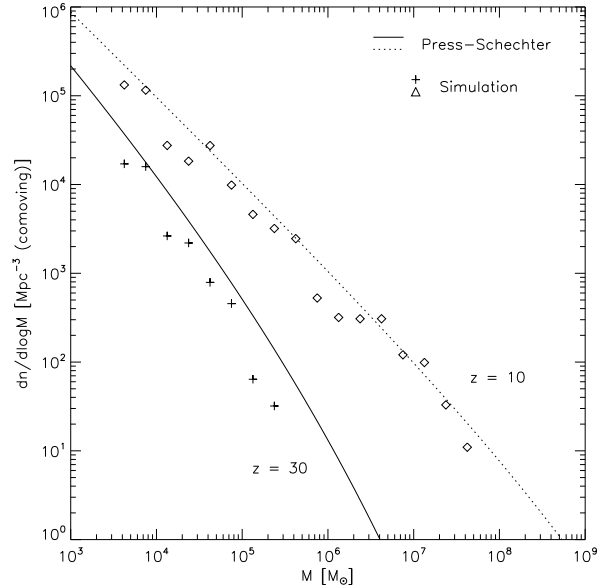


Figure 1. Comparison of the Press-Schechter mass function (solid and dotted line) and the simulation results (crosses and triangles) at $z \simeq 30$ (lower set) and $z \simeq 10$ (upper set). The simulation generally agrees with the analytic prediction, although there is a large scatter due to the finite box size. The expected number of atomic cooling haloes per cubic Mpc (comoving) at $z \simeq 10$ is of order 10.

into the galaxy delineated by the insets in the right panels of Fig. 2 and further enlarged in Figs. 8, 9, 10 and 12. Although this structure is not yet fully virialized and exhibits a number of sub-components, it has a common potential well and attracts gas from the IGM towards its center of mass, where it is accreted by the central BH once it falls below the Bondi radius. The virial temperature of the first minihalo increases according to equation (2) until it reaches $\simeq 10^4$ K and atomic cooling sets in, at which point the equation of state softens and a fraction of the potential energy is converted into kinetic energy. Star formation takes place only in the most massive minihaloes, with 10 Pop III.1 star formation sites residing in the volume that is destined to form the galaxy. This has important consequences for the role of stellar feedback, and will be further discussed in Section 4. The morphology of the galaxy can best be seen in Fig. 3, where we show a three-dimensional rendering of the central 150 kpc (comoving), i.e. the same field of view as in Fig. 2. The temperature is colour-coded such that the hottest regions with $T \simeq 10^4$ K are displayed in bright red. Here, the true spacial structure of the galaxy becomes more apparent, showing that its environment is organized into prominent filaments with a high amount of substructure. In some instances, star-forming minihaloes have aligned along these filaments and will soon merge with the galaxy.

3.4 Merger Tree

The hierarchical assembly of the galaxy can be best described by means of a merger tree that depicts the evolution of all progenitor haloes. We construct such a merger tree by tagging all DM particles that reside in the parent atomic

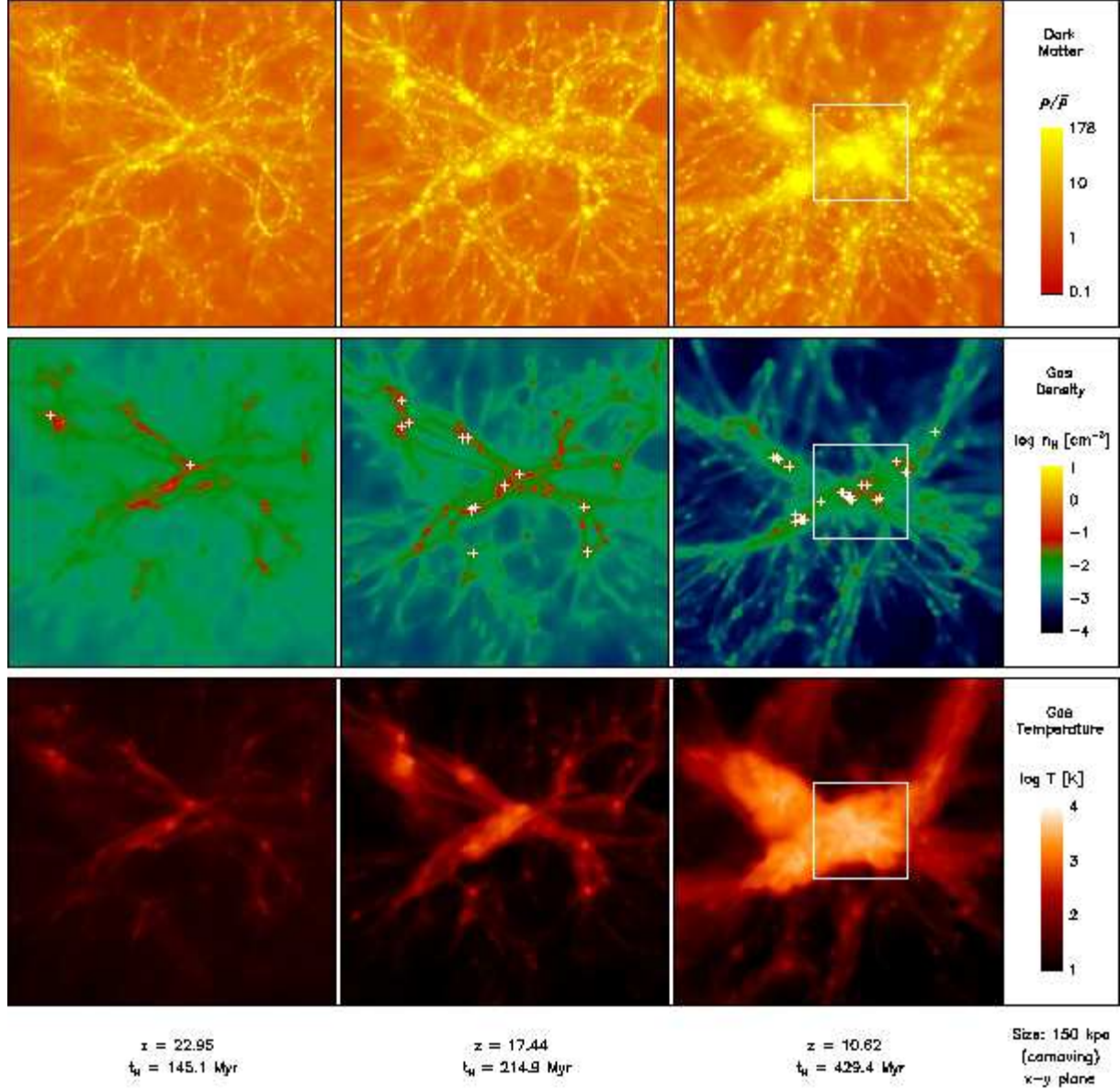


Figure 2. The DM overdensity, hydrogen number density and temperature averaged along the line of sight within the central $\simeq 150$ kpc (comoving) at three different output times, from $z \simeq 23$, when the first star-forming minihalo at the center of the box collapses, to $z \sim 10$, when the first galaxy forms. White crosses denote Pop III.1 star formation sites in minihaloes, and the insets approximately delineate the boundary of the galaxy, further enlarged in Figs. 8, 9, 10 and 12. *Top row:* The hierarchical merging of DM haloes leads to the collapse of increasingly massive structures, with the least massive progenitors forming at the resolution limit of $\simeq 10^4 M_\odot$ and ultimately merging into the first galaxy with $\simeq 5 \times 10^7 M_\odot$. The brightest regions mark haloes in virial equilibrium according to the commonly used criterion $\rho/\bar{\rho} > 178$. Although the resulting galaxy is not yet fully virialized and is still broken up into a number of sub-components, it shares a common potential well and the infalling gas is attracted towards its center of mass. *Middle row:* The gas generally follows the potential set by the DM, but pressure forces prevent collapse in haloes below $\simeq 2 \times 10^4 M_\odot$ (cosmological Jeans criterion). Moreover, star formation only occurs in haloes with virial masses above $\simeq 10^5 M_\odot$, as densities must become high enough for molecule formation and cooling. *Bottom row:* The virial temperature of the first star-forming minihalo gradually increases from $\simeq 10^3$ K to $\simeq 10^4$ K, at which point atomic cooling sets in.

cooling halo and track their location backwards in time. If they are part of a group at a previous timestep, they are considered to reside in a halo with mass equal to the sum of their individual masses. We repeat this process until all tagged particles are no longer part of a group or the mass falls below the resolution limit. Fig. 4 shows the resulting absolute and differential mass growth of the galaxy. Accre-

tion is fueled by minor as well as major mergers, with the latter showing the tendency to double the mass of the halo. In the course of $\simeq 400$ Myr, the accretion rate increases from $\simeq 5 \times 10^{-3} M_\odot \text{ yr}^{-1}$ to $\simeq 0.5 M_\odot \text{ yr}^{-1}$, but varies significantly in between due to the highly complex nature of bottom-up structure formation.

To illustrate the substantial degree of complexity in-

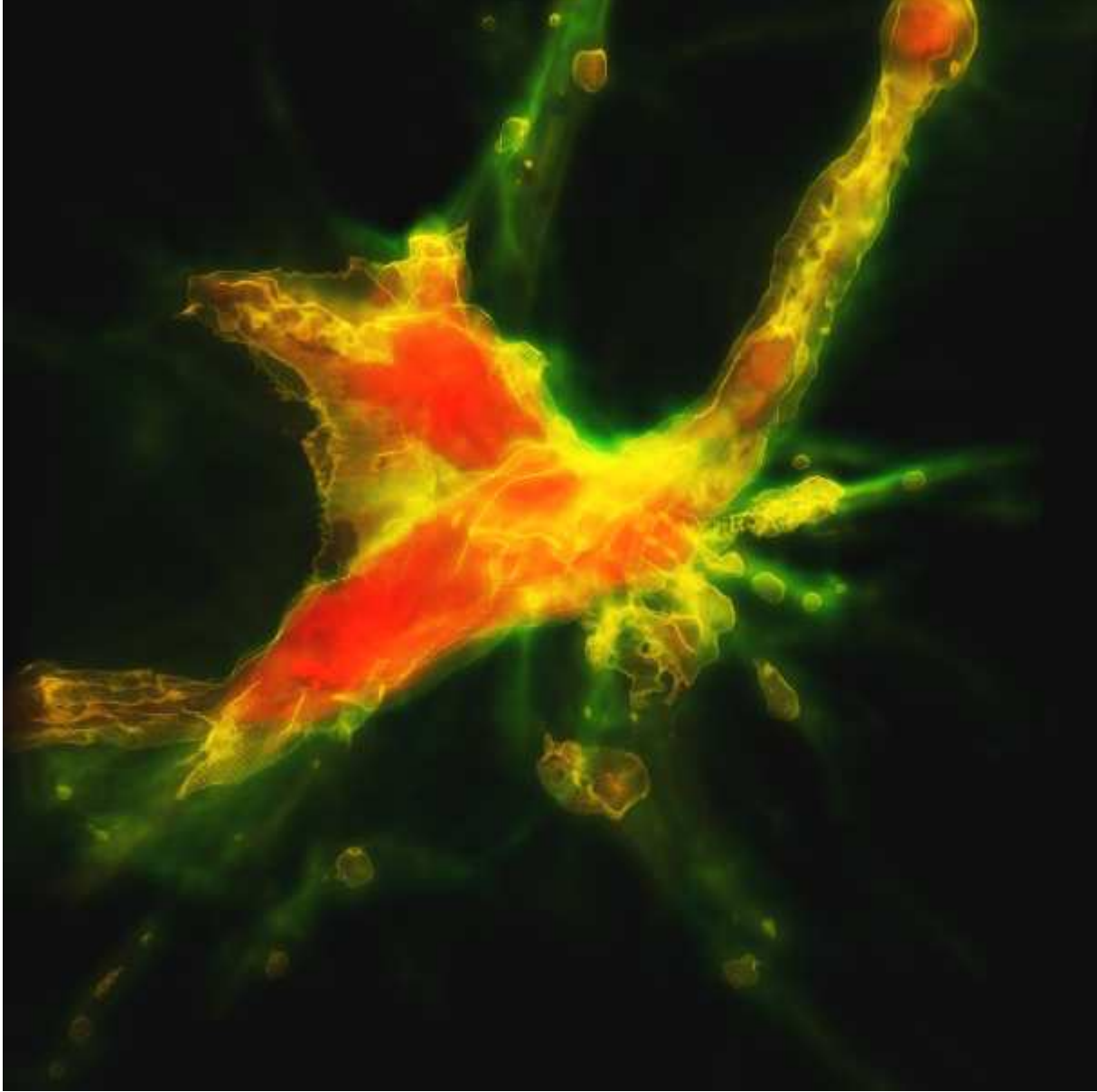


Figure 3. A three-dimensional rendering of the central $\simeq 150$ kpc (comoving), showing the same field of view as in Fig. 2. The temperature is colour-coded such that the hottest regions with $T \simeq 10^4$ K are displayed in bright red. Here, the true spacial structure of the galaxy becomes more clear, showing that its environment is organized into prominent filaments with a high amount of substructure. In some instances, star-forming minihaloes have aligned along these filaments and will soon merge with the galaxy.

involved, Fig. 5 shows the individual paths of all progenitor haloes down to the DM resolution limit of $\simeq 10^4 M_\odot$. The initial widening of the tree indicates that an increasing number of minihaloes collapse, while at $z \simeq 20$ merging becomes dominant and the degree of complexity decreases again. The timescale for the widening of the tree is $\simeq 150$ Myr, while the completion of the merging process requires another $\simeq 250$ Myr. The total number of haloes above $\simeq 10^4 M_\odot$ that merge to form the galaxy is $\simeq 300$. A more sophisticated analysis of the merging process is presented in Fig. 6, where the individual paths and masses of all progenitor haloes are shown. Each line represents an individual halo, while the colour denotes its mass. The target halo seeding the first galaxy is indicated by the right-most

path. Sites of Pop III.1 star formation are denoted by star symbols, and the oval denotes the formation of the atomic cooling halo. The history of this most basic building block of galaxy formation is highly complex, further complicated by the formation of 10 Pop III.1 stars prior to its assembly. However, this is an upper limit on previous star formation activity as we do not include radiative and SN-driven feedback, which would likely reduce the net star formation rate.

The presence of DM fluctuations on mass scales below our resolution limit might imply that Pop III star formation takes place in haloes with viral mass well below $\simeq 2 \times 10^4 M_\odot$, but pressure forces prevent gas from settling into these shallow potential wells (cosmological Jeans criterion). Moreover, gas may not be able to collapse beyond the

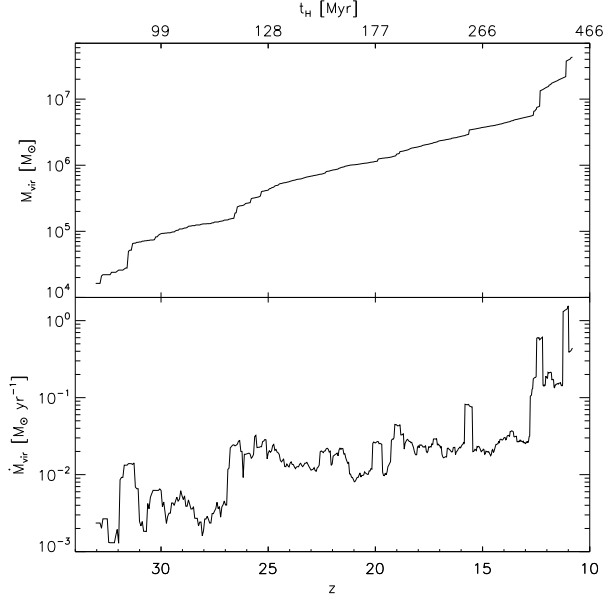


Figure 4. The virial mass (top panel) and accretion rate (bottom panel) of the galaxy as a function of redshift. The growth of the underlying DM halo is fueled by minor as well as major mergers, with the latter showing the tendency to double the mass of the target halo. At $z \simeq 10$, the atomic cooling criterion is fulfilled and a galaxy is born.

point of virialization in $\lesssim 10^5 M_\odot$ haloes, as temperatures and densities do not become high enough for efficient H_2 formation. Dynamical heating by mergers counteracts cooling and thus only a fraction of all minihaloes will be able to form stars (Yoshida et al. 2003). To ascertain the importance of this effect, we determine the masses of all minihaloes experiencing star formation. As described in Section 2, the formation of a Pop III.1 star is denoted by the creation of a sink particle once the hydrogen number density exceeds $\simeq 10^4 \text{ cm}^{-3}$. We implicitly assume that such a parcel of gas does not experience further subfragmentation. With this prescription, we find the following virial masses for all star-forming minihaloes shown in Fig. 6, from top to bottom: $M_{\text{vir}} \simeq [5.8, 1.6, 7.5, 3.5, 4.3, 1.4, 3.2, 9.3, 1.4, 11.8] \times 10^5 M_\odot$. As expected, their masses are in the range $\simeq 10^5 - 10^6 M_\odot$, emphasizing the influence of dynamical heating on haloes below $\simeq 10^9 M_\odot$. Interestingly, the fact that only a fraction of all minihaloes forms stars ensures a constant inflow of cold gas into existing haloes, which is crucial for the growth of the BHs at their centers.

4 COOLING AND STAR FORMATION

A crucial issue concerning the formation of the first galaxies is the chemical and thermal evolution of accreted gas, which ultimately determines the mode of star formation. We here briefly discuss radiative and SN-driven feedback exerted by the very first stars, followed by a discussion of the chemistry and cooling properties of an atomic cooling halo and the implications for second-generation star formation.

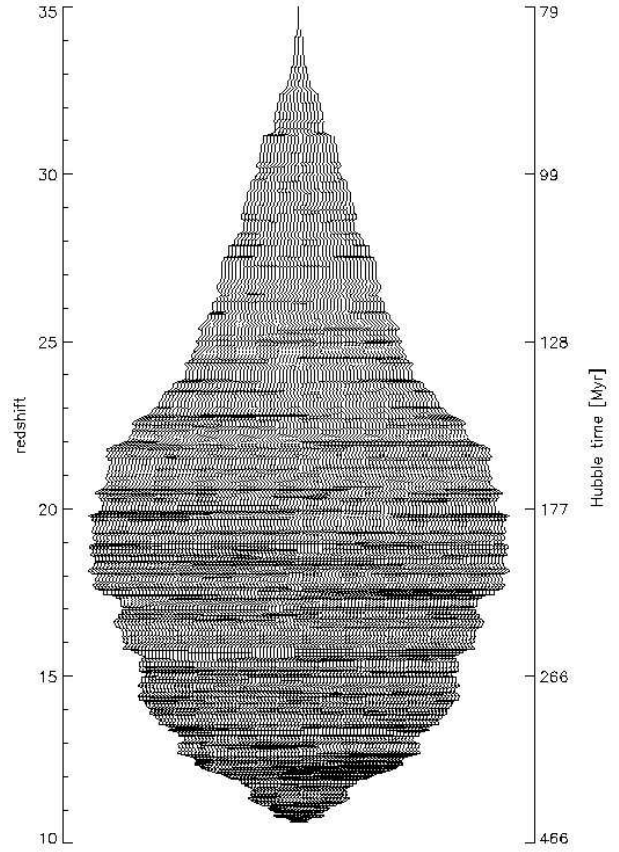


Figure 5. The merger tree of the galaxy, illustrating its complexity as a function of time. New branches indicate the formation of DM haloes at the resolution limit of $\simeq 10^4 M_\odot$. The widening of the tree increases as more and more haloes collapse, until merging dominates and the degree of complexity decreases again. The timescale for the former is $\simeq 150 \text{ Myr}$, while the completion of the merging process requires another $\simeq 250 \text{ Myr}$. A total of $\simeq 300$ haloes above $\simeq 10^4 M_\odot$ merge to form the galaxy.

4.1 Population III.1

As shown in Section 3, star formation ensues in minihaloes before the larger potential wells of the first galaxies assemble. This implies that radiative and SN-driven feedback influences star formation in other minihaloes as well as second-generation star formation in the resulting atomic cooling halo. However, recent numerical simulations have shown that local radiative feedback via photoheating and LW radiation may not be as important as previously thought (Ahn & Shapiro 2007; Johnson et al. 2007a; Whalen et al. 2007), and that a global LW background may only reduce the number of Pop III.1 stars by ~ 50 per cent (Greif & Bromm 2006; Johnson et al. 2007b). An unknown fraction of these stars end their lives as energetic SNe and enrich the surrounding IGM to well above the critical metallicity (Bromm et al. 2003; Greif et al. 2007; Wise & Abel 2007c), while others collapse directly to BHs and do not expel any metals (Heger & Woosley 2002; Heger et al. 2003). Since the timescale for the recollapse of enriched gas is $\gtrsim 100 \text{ Myr}$ (Greif et al. 2007), and mixing is inefficient with

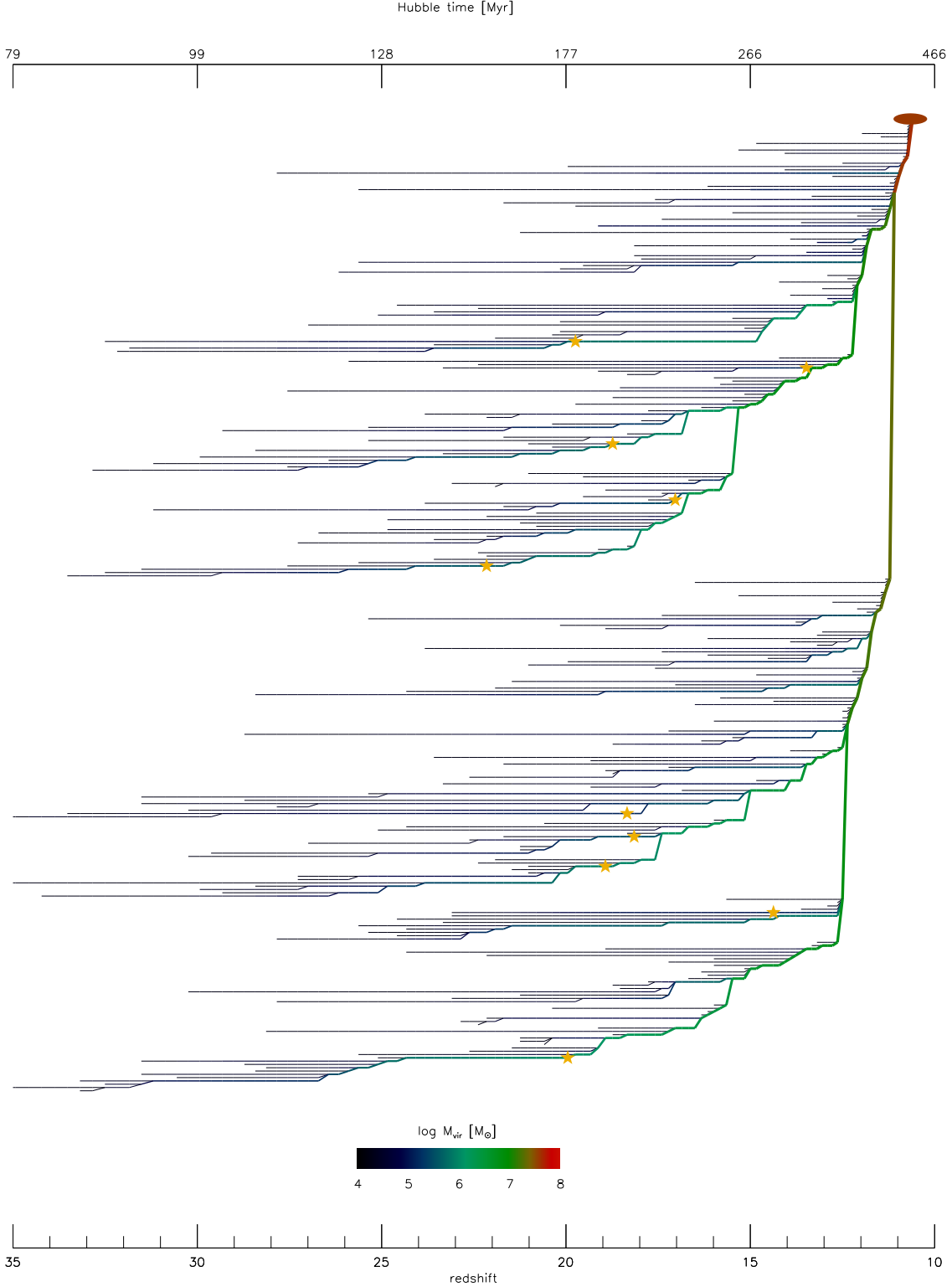


Figure 6. The full merger tree of the galaxy assembling at $z \simeq 10$. Each line represents an individual progenitor halo and is colour-coded according to its mass. The target halo seeding the galaxy is represented by the right-most path, which ultimately attains $\simeq 5 \times 10^7 M_{\odot}$ and fulfils the atomic cooling criterion (denoted by the red oval). Star symbols denote the formation of Pop III.1 stars in minihaloes, showing that in our specific realization 10 Pop III.1 stars form prior to the assembly of the galaxy. Only a fraction of all minihaloes form stars, as dynamical heating via mergers partially offset cooling. Depending on the detailed merger history, this ensures that star-forming minihaloes are supplied with cold gas, which is crucial for the growth of the BHs at their centers.

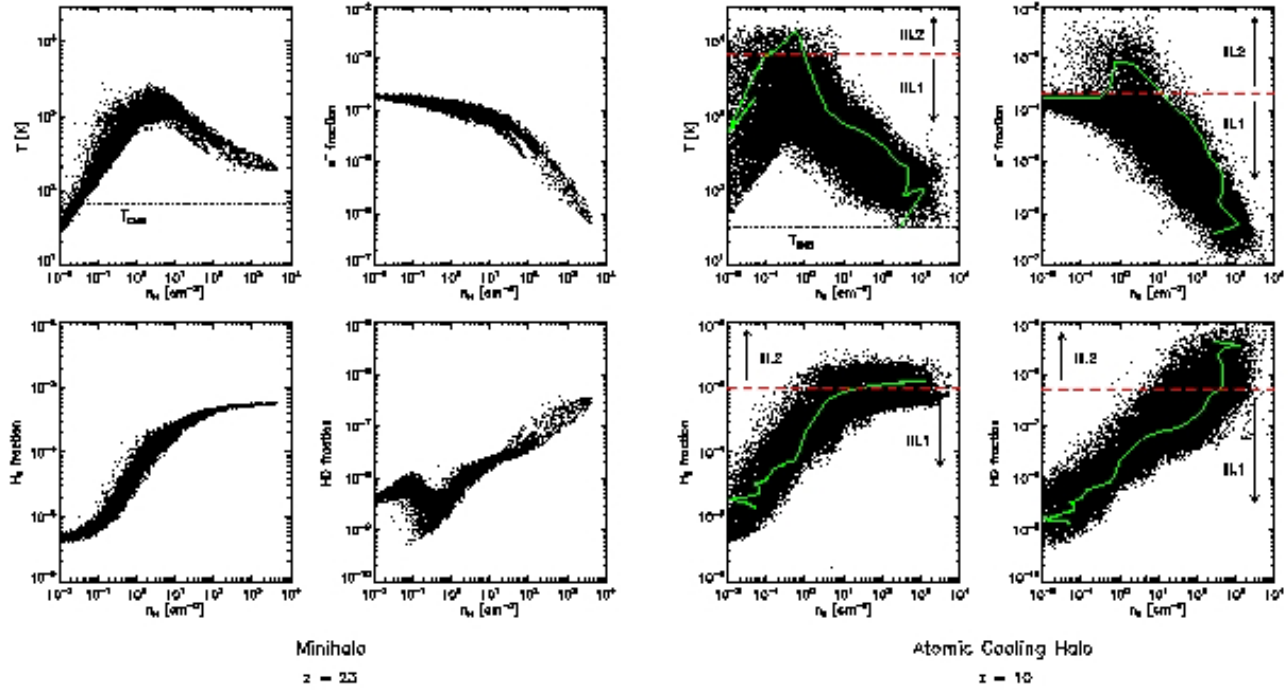


Figure 7. The phase-space distribution of gas inside the first star-forming minihalo (left panel) and the atomic cooling halo (right panel). We show the temperature, electron fraction, HD fraction and H_2 fraction as a function of hydrogen number density, clockwise from top left to bottom left. *Left panel:* In the minihalo case, adiabatic collapse drives the temperature to $\gtrsim 10^3$ K and the density to $n_{\text{H}} \gtrsim 1 \text{ cm}^{-3}$, where molecule formation sets in allowing the gas to cool to $\simeq 200$ K. At this point the central clump becomes Jeans-unstable and ultimately forms a Pop III.1 star. *Right panel:* In the first galaxy, a second cooling channel has emerged due to an elevated electron fraction at the virial shock, which in turn enhances molecule formation and allows the gas to cool to the temperature of the CMB. The dashed red lines and arrows approximately delineate the resulting Pop III.1 and Pop III.2 channels, while the solid green lines denote the path of a representative fluid element that follows the Pop III.2 channel.

respect to pre-established overdensities (Cen & Riquelme 2008), subsequent star formation in minihaloes prior to the assembly of the atomic cooling halo likely remains metal-free. It is much more difficult, however, to predict the character of star formation inside the first galaxies. In the following, we will first examine the consequences of pristine gas collapsing in the atomic cooling halo, and subsequently briefly address the corresponding case of pre-enriched gas.

4.2 Population III.2

The possible existence of a distinct population of metal-free stars in regions of previous ionization has attracted increasing attention (Mackey et al. 2003; Greif & Bromm 2006; Johnson & Bromm 2006; Yoshida 2006; Tan & McKee 2007; Yoshida et al. 2007; but see Ripamonti 2007; McGreer & Bryan 2008). According to theory, an elevated electron fraction catalyzes the formation of H_2 and HD well above the level found in minihaloes and enables the gas to cool to the temperature of the CMB. This reduces the Bonnor-Ebert mass by almost an order of magnitude and likely leads to the formation of Pop III.2 stars with $\gtrsim 10 M_{\odot}$ (Johnson & Bromm 2006). Numerical simulations of star formation in relic H II regions have largely confirmed this picture (Johnson et al. 2007a; Yoshida et al. 2007), while its relevance during the virialization of the first galaxies

has not yet been established (but see Greif & Bromm 2006; Johnson et al. 2007b).

The chemistry of gas contracting in an atomic cooling halo is fundamentally different from that in minihaloes. The latter maintain a primordial electron fraction of $\simeq 3 \times 10^{-4}$ and form a limited amount of molecules, while the virial temperature in an atomic cooling halo exceeds $\simeq 10^4$ K and the elevated electron fraction facilitates the formation of high H_2 and HD abundances. This allows the gas to cool to the temperature of the CMB instead of the canonical $\simeq 200$ K found in minihaloes. In the left panel of Fig. 7, we show the properties of the gas in the first star-forming minihalo at the center of the computational box. The primordial electron fraction remains constant until densities become high enough for electron recombination. After adiabatic heating to $\gtrsim 10^3$ K, molecule formation sets in and the gas cools to $\simeq 200$ K, at which point the central clump becomes Jeans-unstable and inevitably forms a Pop III.1 star. In contrast, the right panel of Fig. 7 shows the density and temperature of the gas inside the atomic cooling halo. The conventional H_2 cooling channel is still visible, but a second path from low to high density has emerged, enabled by an elevated electron fraction at the virial shock, which in turn enhances the formation of H_2 and HD and allows the gas to cool to the temperature of the CMB. The dashed red lines and black arrows in Fig. 7 approximately delineate both channels, showing that the electron fraction in the Pop III.2

case has been elevated by an order of magnitude to $\sim 10^{-3}$, and the H_2 fraction to $\simeq 2 \times 10^{-3}$. As already estimated in Johnson et al. (2007b), the HD fraction grows to above $\simeq 10^{-6}$.

To more clearly illustrate this point, we plot the path of a representative fluid element evolving along the Pop III.2 channel (solid green lines in Fig. 7). Such gas indeed cools to the CMB floor, potentially enabling the formation of Pop III.2 stars. The mass fraction entering this channel is relatively low at the time considered here since the atomic cooling threshold has just been surpassed, but should quickly rise as freshly accreted material is shock-heated to $\simeq 10^4$ K. We cannot study any possible fragmentation, since the gas rapidly falls to within the Bondi radius of the central BH, and is thus accreted by the sink particle. It will be very interesting to investigate the fragmentation of the Pop III.2 mode in future, higher-resolution simulations, in particular testing the predicted mass scale of $\gtrsim 10 M_\odot$ (see, e.g. Clark et al. 2008).

What are the implications of this result? Parcels of gas that are accreted onto the galaxy through the virial shock can cool to the temperature of the CMB and possibly become gravitationally unstable, resulting in the formation of Pop III.2 stars. Including radiative feedback from previous star formation would only strengthen this conclusion, as the degree of ionization would be increased even further (Wise & Abel 2007c). As long as the gas collapsing into the first galaxies remains pristine, primordial star formation will therefore likely be dominated by intermediate-mass (Pop III.2) stars (Greif & Bromm 2006). The crucial question, however, is: Can the gas inside the first galaxies remain metal-free?

4.3 Population II

In the previous sections, we have found that of order 10 Pop III.1 stars form prior to the assembly of the atomic cooling halo. In this case it appears unlikely that all of them will collapse into BHs without any metal-enrichment (Johnson et al. 2007b). Even a single SN from a massive Pop III star would already suffice to reach levels above the critical metallicity, at least on average (Bromm et al. 2003; Greif et al. 2007; Wise & Abel 2007c). More generally, at some stage in cosmic history, there must have been a transition from primordial, high-mass star formation to the ‘normal’ mode that dominates today. The discovery of extremely metal-poor stars in the Galactic halo with masses below one solar mass (Christlieb et al. 2002; Frebel et al. 2005; Beers & Christlieb 2005) indicates that this transition occurs at abundances considerably smaller than the solar value. At the extreme end, these stars have iron abundances less than 10^{-5} times the solar value, but show significant carbon and oxygen enhancements, which could be due to unusual abundance patterns produced by enrichment from BH-forming Pop III SNe (Umeda & Nomoto 2003), or due to mass transfer from a close binary companion, whose frequency is predicted to increase with decreasing metallicity (Lucatello et al. 2005).

Identifying the critical metallicity at which this transition occurs is subject to ongoing research. One approach is to argue that low mass star formation becomes possible only when atomic fine-structure line cooling from

carbon and oxygen becomes effective (Bromm et al. 2001; Bromm & Loeb 2003b; Santoro & Shull 2006; Frebel et al. 2007), setting a value for Z_{crit} at $\simeq 10^{-3.5} Z_\odot$. Another possibility, first proposed by Omukai et al. (2005), is that low mass star formation is a result of dust-induced fragmentation occurring at high densities, $n_{\text{H}} \simeq 10^{13} \text{ cm}^{-3}$, and thus at a very late stage in the protostellar collapse. In this model, $10^{-6} \lesssim Z_{\text{crit}} \lesssim 10^{-5} Z_\odot$, where much of the uncertainty in the predicted value results from uncertainties in the dust composition and the degree of gas-phase depletion (Schneider et al. 2002, 2006). Recent numerical simulations by Tsuribe & Omukai (2006) as well as Clark et al. (2008) provide support for this picture. However, the existing data of metal-poor Galactic halo stars seems to be well accommodated by the C and O based fine-structure model (Frebel et al. 2007).

In the present simulation, we do not follow the metallicity evolution of the infalling gas. Thus, we can only speculate about the properties of the resulting stellar population. It appears reasonable to assume that some of the accreting material is still pristine and free of metals, triggering the formation of lower-mass metal-free Pop III.2 stars. Gas that flows in at even later times may already have experienced metal enrichment from previous Pop III SNe in nearby minihaloes. Because of the high level of turbulence within the virial radius at that time (see Section 5), the incoming new material is likely to efficiently mix with the pre-existing zero-metallicity gas and the era of Pop III star formation could come to an end. This transition possibly occurs at the same time as the onset of significant degrees of turbulence in the atomic cooling halo. We therefore speculate that some of the extremely metal-deficient stars in the halo of the Milky Way may have formed as early as redshift $z \simeq 10$ (Clark et al. 2008).

5 TURBULENCE

The development of turbulence in gas flowing into the central potential well of the halo strongly influences its fragmentation behaviour and consequently its ability to form stars. Detailed studies of the interstellar medium in the Milky Way, for instance, tell us that turbulence determines when and where star formation occurs and that it is the intricate interplay between gravity on the one hand, and turbulence, thermal pressure and magnetic fields on the other that sets the properties of young stars and star clusters (Larson 2003; Mac Low & Klessen 2004; Ballesteros-Paredes et al. 2007). In the context of our work, we investigate the velocity field and energy distribution that builds up during the assembly of the galaxy. As opposed to cooling flows in low-mass haloes, the accretion flow onto the deep central potential well of the atomic cooling halo considered here becomes highly turbulent within the virial radius.

5.1 The Development of Turbulence: Hot vs. Cold Accretion

One of the most important consequences of atomic cooling is the softening of the equation of state below the virial radius, allowing a fraction of the potential energy to be converted into kinetic energy (Wise & Abel 2007b). This im-

plies that perturbations in the gravitational potential can generate turbulent motions on galactic scales, which are then transported to the center of the galaxy. In this context it is important to investigate the accretion of gas onto the galaxy in more detail.

In principle, there are two distinct modes of accretion. Gas accreted directly from the IGM is heated to the virial temperature and comprises the sole channel of inflow until cooling in filaments becomes important. This mode is termed hot accretion, and dominates in low-mass haloes at high redshift. In the atomic cooling halo, the formation of the virial shock and the concomitant heating are visible in Fig. 9, where we show the hydrogen number density and temperature of the central $\simeq 40$ kpc (comoving) around the BH at the center of the galaxy. This case also reveals a second mode, termed cold accretion. It becomes important as soon as filaments are massive enough to enable molecule reformation, which allows the gas to cool and flow into the central regions of the nascent galaxy with high velocities. In Fig. 9, the cold gas accreted along filaments from the left and right is clearly distinguishable from the hot gas at the virial shock. These streams are also visible in Fig. 10, where we compare the radial with the tangential velocity component, and in Fig. 8, where we show the Mach number of infalling gas. Evidently, inflow velocities can be as high as 20 km s^{-1} , with Mach numbers of order 10.

In Fig. 11, we compare the energy distribution and mass fraction of cold ($< 500 \text{ K}$) versus hot ($> 500 \text{ K}$) gas in radial shells for the first star-forming minihalo just before the formation of the sink particle, and the atomic cooling halo assembling at $z \simeq 10$. The blue, green and red lines denote the azimuthally averaged ratio of radial, tangential and thermal to potential energy, respectively. The black lines show the sum of all three components, and the dotted lines indicate the ratio required for perfect virialization. In the minihalo case, the total energy is dominated by thermal energy, although its share decreases towards the center where cooling via molecular hydrogen becomes important. The radial kinetic energy dominates over the tangential component down to $r_{\text{tan}} \simeq 5 \text{ pc}$, where the mass fraction of cold gas rapidly rises and the cloud becomes rotationally supported. Efficient cooling implies that the total energy drops below that required for perfect virialization.

In the atomic cooling halo, the total energy at $r_{\text{vir}} \simeq 1 \text{ kpc}$ is dominated by bulk radial motions. The distinction between hot and cold gas in the right panels of Fig. 11 shows that a large fraction of the kinetic energy injected into the galaxy comes from cold gas accreted along filaments, even though its mass fraction is initially small. The energy in tangential motions begins to dominate at $r_{\text{tan}} \simeq 200 \text{ pc}$, showing that the radial energy of the cold gas flowing in along filaments is converted into turbulent motions. This is fundamentally different from the collapse of gas in minihaloes, where the radial energy is converted into a directed rotation along a single axis. The distinct features at $r \simeq 350 \text{ pc}$ are caused by a subhalo that has not yet merged with the central clump (see also Figs. 2 and 3). Once again, the total energy budget falls below that required for perfect virialization, as atomic hydrogen as well as molecular cooling are able to radiate away a significant fraction of the potential energy released. We conclude that the high energy input by cold accretion is ideally suited to drive turbulence at the

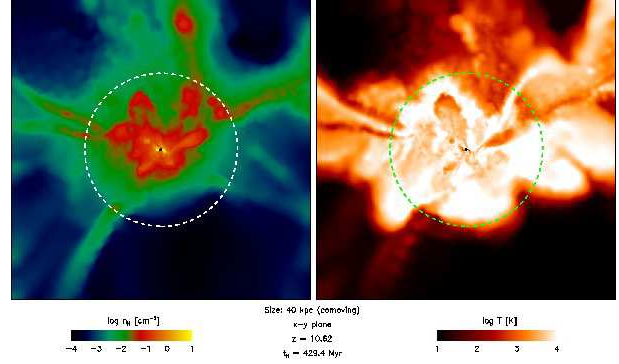


Figure 8. The central $\simeq 40$ kpc (comoving) of the computational box, roughly delineated by the insets in Fig. 2. Shown is the Mach number in a slice centered on the BH at the center of the galaxy, indicated by the filled black circle. The dashed line denotes the virial radius at a distance of $\simeq 1 \text{ kpc}$. The Mach number approaches unity at the virial shock, where gas accreted from the IGM is heated to the virial temperature over a comparatively small distance. Inflows of cold gas along filaments are supersonic by a factor of $\simeq 10$ and generate a high amount of turbulence at the center of the galaxy, where typical Mach numbers are between 1 and 5.

center of the galaxy, where bulk radial inflows are converted into turbulent motions on small scales.

5.2 Shocks and Fragmentation Properties

Shock fronts can arise where supersonic flows experience sudden deceleration and, if unorganized, indicate the presence of supersonic turbulence. As discussed above, cold accretion is a viable agent for driving turbulence, due to the prodigious amount of momentum and kinetic energy it brings to the center of the galaxy. In Fig. 12, we show the divergence and vorticity of the velocity field during the virialization of the galaxy. A comparison with Fig. 8 implies that there are indeed regions of supersonic flow that experience rapid deceleration and form shocks. In our case, two physically distinct mechanisms are responsible for creating these shocks. The virial shock forms where the ratio of infall velocity to local sound speed approaches unity, and is clearly visible in the left panel of Fig. 12. The velocity divergence is negative since the gas rapidly decelerates, while the vorticity is almost negligible. In contrast, the unorganized multitude of shocks that form near the center of the galaxy are mostly caused by accretion of cold, high-velocity gas from filaments. These are more pronounced than the virial shock and have a significantly higher angular component. They create transitory density perturbations that could in principle become Jeans-unstable and trigger the gravitational collapse of individual clumps.

How does the turbulence generated in the infalling material influence its fragmentation behaviour and control subsequent star formation? From detailed observational and theoretical studies of star formation in our Milky Way we know that turbulence plays a pivotal role in the formation of stars and star clusters. It is usually strong enough to counterbalance gravity on global scales. By the same token, however, it will usually provoke collapse locally. Turbulence establishes a complex network of interacting shocks, where

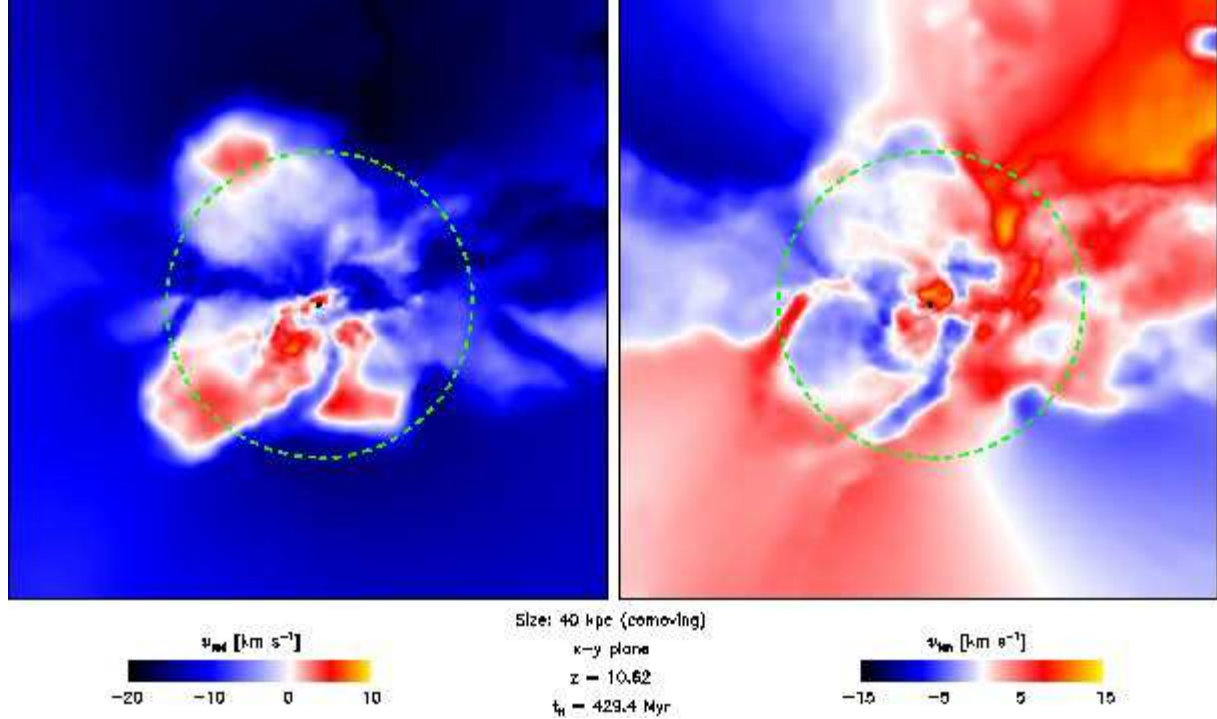


Figure 9. The central $\simeq 40$ kpc (comoving) of the computational box, roughly delineated by the insets in Fig. 2. Shown is the hydrogen number density (left panel) and temperature (right panel) in a slice centered on the BH at the center of the galaxy, indicated by the filled black circle. The dashed lines denote the virial radius at a distance of $\simeq 1$ kpc. Hot accretion dominates where gas is accreted directly from the IGM and shock-heated to $\simeq 10^4$ K. In contrast, cold accretion becomes important as soon as gas cools in filaments and flows towards the center of the galaxy, such as the streams coming from the left- and right-hand side. They drive a prodigious amount of turbulence and create transitory density perturbations that could in principle become Jeans-unstable. In contrast to minihaloes, the initial conditions for second-generation star formation are highly complex, with turbulent velocity fields setting the fragmentation properties of the gas.

regions of high density build up at the stagnation points of convergent flows. To result in the formation of stars, local collapse must progress to high enough densities on time scales shorter than the typical interval between two successive shock passages. Only then can the collapsing core decouple from the ambient flow pattern and build up a star. The accretion flow onto these objects and consequently the final stellar mass strongly depends on the properties of the surrounding turbulent flow.

In concert with the thermodynamic properties of the gas, leading to the cooling of high-density material to the CMB limit (see Section 4), length scale and strength of the turbulence are the most important parameters governing its fragmentation behaviour and consequently the properties of star formation, such as its timescale and overall efficiency (Klessen et al. 2000; Vázquez-Semadeni et al. 2003; Krumholz & McKee 2005). In the atomic cooling halo discussed here, this will eventually lead to the transition to Pop II star formation. However, a quantitative understanding of the fragmentation behaviour of the turbulent gas would require dedicated high-resolution simulations, which is beyond the scope of this work.

6 MASSIVE BLACK HOLE GROWTH

Galaxy formation in general involves the co-evolution of a central black hole and the surrounding stellar system, the

one influencing the other. Two crucial unsolved problems are: What were the seeds for BH growth, and how important was this co-evolution at very high redshifts? We here begin to address these questions. Different scenarios have been suggested to account for the seeds of BH growth (Rees 1984): the direct collapse of gas in atomic cooling haloes in the presence of a strong photodissociating background, or stellar remnants of massive, metal-free stars. In the following, we discuss the latter possibility and investigate the growth of a MBH forming at the center of the galaxy.

6.1 Accretion Rate

Even though studies of stellar evolution have shown that primordial stars may explode as energetic SNe, we here assume that all Pop III.1 stars collapse directly to BHs (Heger & Woosley 2002; Heger et al. 2003). Their initial mass is dictated by the resolution limit to $M_{\text{BH}} \simeq 2 \times 10^3 M_{\odot}$, with accretion onto the BH governed by the criteria discussed in Section 2. Recent investigations have shown that photoheating by the progenitor star can delay efficient accretion by reducing the central density to $\lesssim 1 \text{ cm}^{-3}$ (Johnson & Bromm 2007). However, the suppression of accretion also depends on the detailed merger history of the host halo. For example, a major merger occurring just after the formation of the BH could transport enough cold gas to its center to enable accretion at the Eddington rate. As

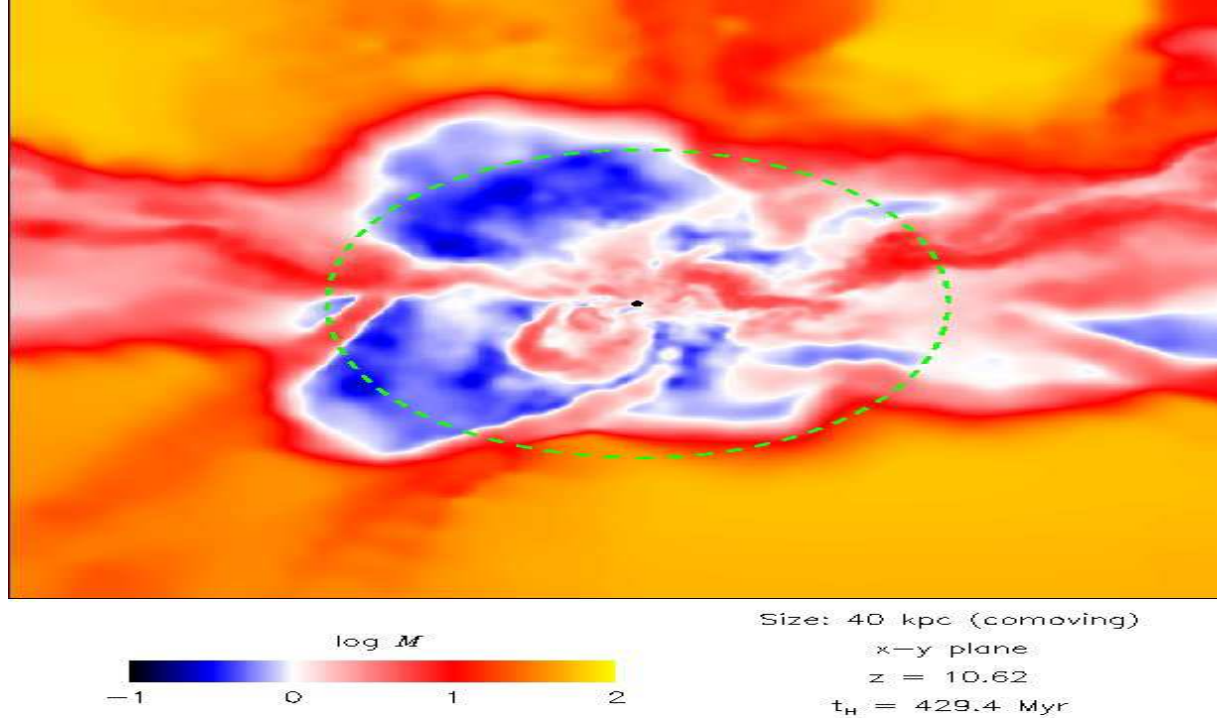


Figure 10. The central $\simeq 40$ kpc (comoving) of the computational box, roughly delineated by the insets in Fig. 2. Shown is the radial (left panel) and tangential velocity in the x-y plane (right panel) in a slice centered on the BH at the center of the galaxy, indicated by the filled black circle. The dashed lines denote the virial radius at a distance of $\simeq 1$ kpc. Streams of cold gas from filaments, such as those coming from the left- and right-hand side, are clearly visible and can have velocities of up to 20 km s^{-1} . Some even penetrate the center and create regions of positive radial velocities. Angular velocities are particularly high towards the center of the galaxy, where bulk radial inflows are converted into turbulent motions on small scales. The presence of flows in both directions imply that these are unorganized instead of coherently rotating, such as is the case in minihaloes (see also Fig. 11).

shown in Fig. 6, some minihaloes merge shortly after forming a BH, in some cases after only a few million years. On the other hand, if mergers are absent or incoming haloes are not sufficiently massive, accretion could be suppressed for $\gtrsim 100$ Myr (Johnson & Bromm 2007). In our approach to derive an upper limit on the accretion rate, we neglect the effects of photoheating by the progenitor star such that accretion is governed solely by the supply of cold gas brought to the center of the halo.

A more precise modeling would also require a prescription for radiation emitted by the BH-powered miniquasar and its feedback on the surrounding disk (Volonteri & Rees 2006). In a simpler approach, one can assume a given radiative efficiency ϵ , which denotes the ratio of BH luminosity to accreted mass energy, and assume that accretion is spherically symmetric. This leads to the Eddington accretion rate:

$$\dot{M}_{\text{Edd}} = \frac{1}{\epsilon} \frac{M_{\text{BH}}}{t_{\text{Salp}}}, \quad (3)$$

where t_{Salp} is the Salpeter time, defined by:

$$t_{\text{Salp}} = \frac{c\sigma_{\text{T}}}{4\pi G m_{\text{H}}} \simeq 450 \text{ Myr}. \quad (4)$$

The mass of the BH as a function of time is thus given by:

$$M_{\text{BH}}(t) = M_{\text{BH}}(t_0) \exp\left(\frac{1-\epsilon}{\epsilon} \frac{t-t_0}{t_{\text{Salp}}}\right). \quad (5)$$

In Fig. 13, we compare the mass growth of the most massive BH with the Eddington-limited model, using a fiducial value

of $\epsilon = 1/10$. We find that the accretion rate remains roughly constant at $\simeq 5 \times 10^{-3} M_{\odot} \text{ yr}^{-1}$, such that the BH grows from $\simeq 2 \times 10^3$ to $\simeq 10^6 M_{\odot}$ in the course of $\simeq 300$ Myr. Due to our neglect of radiative feedback, the BH accretes well above the Eddington rate throughout most of its lifetime. At later times the accretion rate stagnates, most likely caused by the high kinetic energy input at the center via cold accretion (see Fig. 11). Consequently, the fraction of unbound gas near the BH increases and its mass growth is slowed. We conclude that Eddington accretion is possible under the most favourable circumstances, e.g. where a recent merger brings an ample supply of cold gas to the center of the halo, but generally radiative feedback by the progenitor star and the disk around the BH will lead to sub-Eddington accretion rates (Johnson & Bromm 2007; Pelupessy et al. 2007).

6.2 Accretion Luminosity

The radiation generated by the BH-powered miniquasar can have numerous effects on the formation of the first galaxies. In addition to its negative feedback on star formation via photoheating, the emitted radiation can contribute to the LW background, as well as to the reionization of the Universe (Madau & Quataert 2004; Ricotti & Ostriker 2004; Kuhlen & Madau 2005). In the following, we derive an upper limit on the photodissociating flux and the number of ionizing photons emitted by a stellar remnant BH accreting at the Eddington limit.

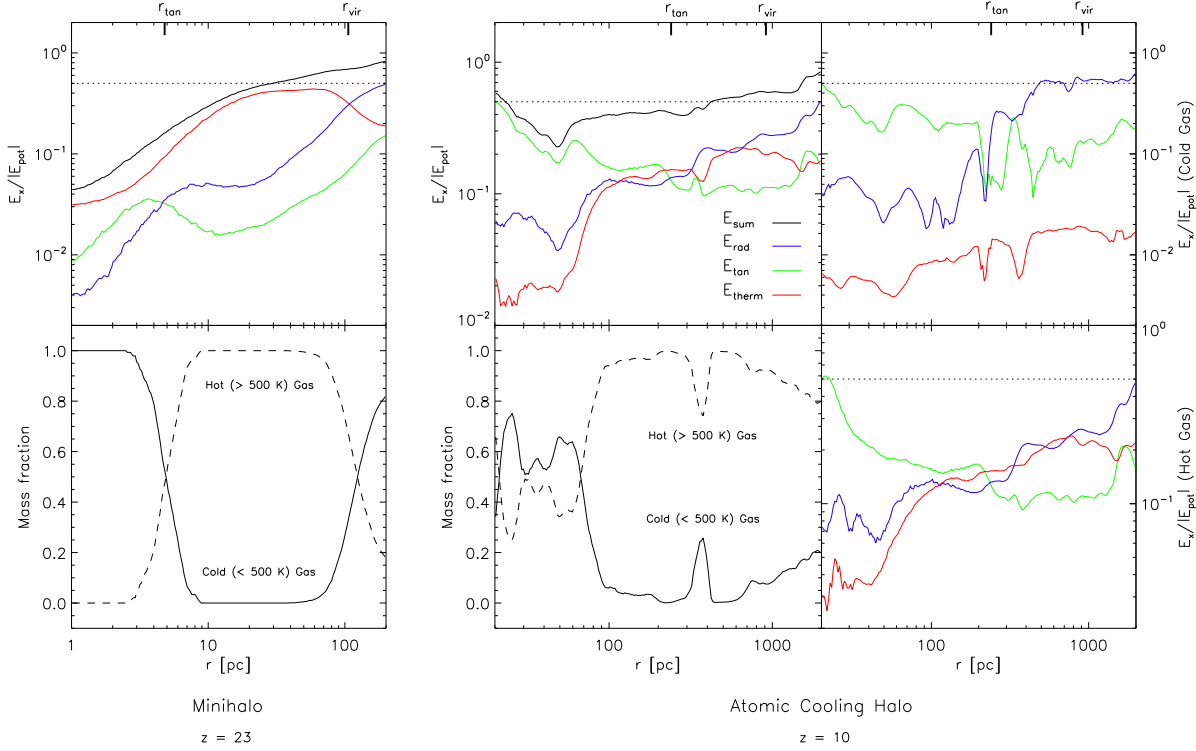


Figure 11. The energy distribution and mass fraction of cold (< 500 K) versus hot (> 500 K) gas in radial shells for the first star-forming minihalo just before the formation of the sink particle, and the atomic cooling halo assembling at $z \simeq 10$. The azimuthally averaged ratio of radial, tangential and thermal to potential energy are shown as blue, green and red lines, respectively. The black lines show the sum of all three components, and the dotted lines indicate the ratio required for perfect virialization. In the minihalo case, the total energy is dominated by thermal energy, although its share decreases towards the center where cooling via molecular hydrogen becomes important. The radial kinetic energy dominates over the tangential component down to $r_{\text{tan}} \simeq 5$ pc, where the mass fraction of cold gas rapidly rises and the cloud becomes rotationally supported. In the atomic cooling halo, the total energy at $r_{\text{vir}} \simeq 1$ kpc is dominated by bulk radial motions. The distinction between hot and cold gas in the right panels shows that most of the kinetic energy injected into the galaxy comes from the cold gas accreted along filaments, even though its mass fraction is initially small. The tangential component begins to dominate at $r_{\text{tan}} \simeq 200$ pc, where the radial flow of cold gas along filaments is converted into turbulent motions. The distinct features at $r \simeq 350$ pc are caused by a subhalo that has not yet merged with the central clump (see also Figs. 2 and 3).

6.2.1 Photodissociating Flux

To determine the flux of LW photons, we first model the temperature profile of the surrounding accretion disk:

$$T(r) = \left(\frac{3}{8\pi} \frac{GM_{\text{BH}} \dot{M}_{\text{BH}}}{\sigma_{\text{SB}} r^3} \right)^{\frac{1}{4}}, \quad (6)$$

where r is the distance from the BH, M_{BH} its mass, \dot{M}_{BH} the accretion rate, and σ_{SB} the Stefan-Boltzmann constant (Pringle 1981). For simplicity, we have taken the disk to be a thin disk, such that each annulus radiates as a blackbody of temperature given by the above equation. The inner-most radius of the disk is given by:

$$r_{\text{inner}} \sim 2 \text{ km} \left(\frac{M_{\text{BH}}}{M_{\odot}} \right), \quad (7)$$

corresponding to a high value for the BH spin parameter $a \gtrsim 0.9$ (Makishima et al. 2000; Vierdayanti et al. 2007), which we expect considering the large angular momentum of the accreted gas (see Fig. 11). We integrate the flux over the surface of the disk from r_{inner} to $r_{\text{outer}} = 10^4 r_{\text{inner}}$, where the contributions to both the photodissociating and ionizing fluxes are negligible. To determine the flux emit-

ted in the LW bands, we evaluate the total emitted flux at 12.87 eV. In the upper panel of Fig. 14, we show the LW flux in units of $10^{-21} \text{ erg s}^{-1} \text{ cm}^{-2} \text{ Hz}^{-1} \text{ sr}^{-1}$ for the case of Eddington-limited accretion at 1 kpc distance from the BH. We consider initial BH masses of 100 and 500 M_{\odot} , roughly the range expected for the direct collapse of massive Pop III stars (Heger & Woosley 2002; Heger et al. 2003). As Fig. 14 shows, J_{LW} can greatly exceed the critical value of $\gtrsim 10^{-2}$ required for the suppression of star formation in minihaloes, which mostly relies on efficient H_2 cooling (Machacek et al. 2001; Yoshida et al. 2003; O’Shea & Norman 2008; Johnson et al. 2007b). Furthermore, even a modest LW flux can dissociate enough H_2 such that HD formation and cooling never becomes important, reducing the temperature to which the gas can cool (Yoshida et al. 2007). The impact on primordial star formation in BH-hosting galaxies might thus be severe even for sub-Eddington accretion rates, implying that this effect must be taken into account in future work.

Another important issue concerns the contribution to the global LW background. We may estimate a maximum global LW background by assuming that each atomic cooling halo at $z \gtrsim 10$ hosts a BH accreting at the Eddington

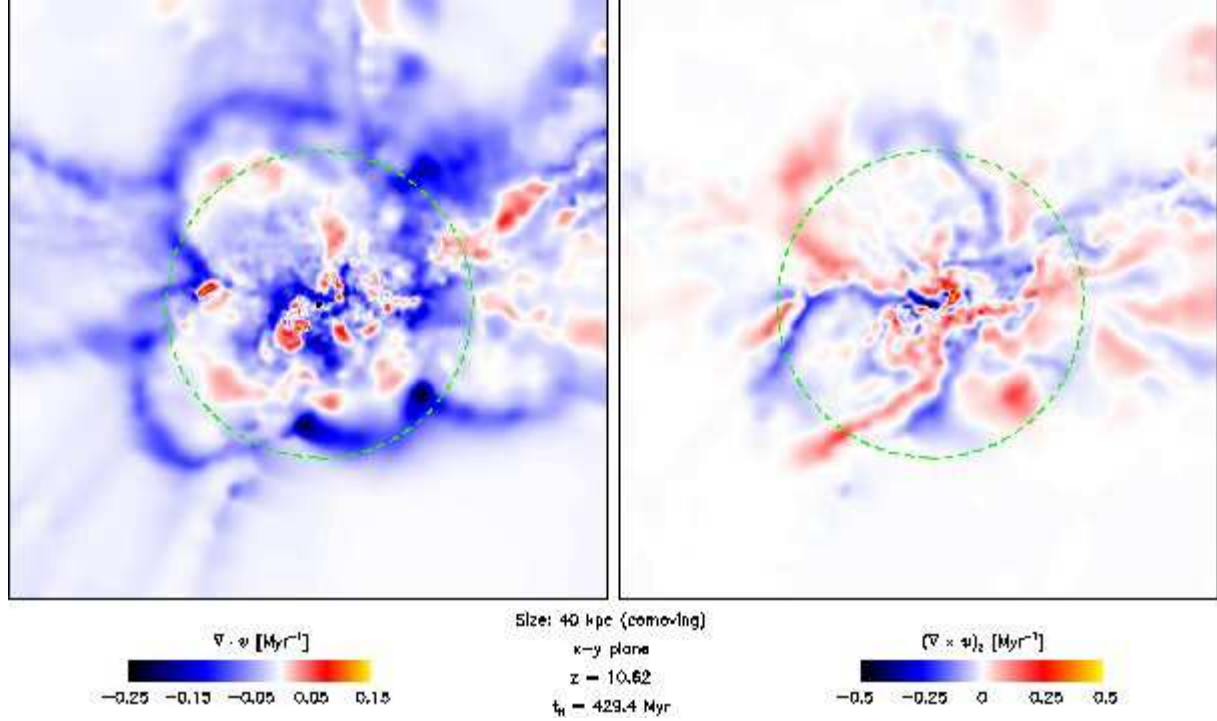


Figure 12. The central $\simeq 40$ kpc (comoving) of the computational box, roughly delineated by the insets in Fig. 2. We show the divergence (left panel) and z-component of the vorticity (right panel) in a slice centered on the BH at the center of the galaxy, indicated by the filled black circle. The dashed lines denote the virial radius at a distance of $\simeq 1$ kpc. The most pronounced feature in the left panel is the virial shock, where the ratio of infall speed to local sound speed approaches unity and the gas decelerates over a comparatively small distance. In contrast, the vorticity at the virial shock is almost negligible. The high velocity gradients at the center of the galaxy indicate the formation of a multitude of shocks where the bulk radial flows of filaments are converted into turbulent motions on small scales.

rate. We can then find an upper limit to the global LW background by summing up the contributions from BHs within a distance equal to the maximum mean free path for a LW photon, $r_{\max} \sim 10$ Mpc at $z = 15$, following the prescription in Johnson et al. (2007b). This estimate yields a maximum global LW background comparable to the LW flux from a single source, as shown in Fig. 14. Such a high flux could have profound consequences for further star formation in minihaloes, but in most cases radiative feedback by the progenitor star will significantly delay accretion, such that a global LW background fueled by accretion onto BHs will likely be subdominant compared to a stellar LW background (Pelupey et al. 2007).

6.2.2 Ionizing Flux

The amount of ionizing radiation released by the accreting BH can be determined in analogy to our calculation of the LW flux. An integration over the temperature profile of the accretion disk yields the total number of hydrogen-ionizing photons emitted per second, shown in the bottom panel of Fig. 14. While massive Pop III stars emit of order 10^{50} hydrogen-ionizing photons per second, these stars live for only $\lesssim 3$ Myr (Bromm et al. 2001; Schaerer 2002). However, as Fig. 14 shows, if Pop III relic BHs are able to accrete efficiently, they may emit 10 – 100 times this number for $\gtrsim 100$ Myr. This enormous flux of ionizing radiation could power H II regions with radii of the order of 10 kpc, larger and longer-lived than the transient H II regions of individ-

ual Pop III stars (Yoshida et al. 2007; Johnson et al. 2007a). Star formation in minihaloes within the H II region could be suppressed if accretion is continuous and drives a persistent radiative flux (Ahn & Shapiro 2007; Whalen et al. 2007). Due to this dramatic radiative feedback associated with high accretion rates, though, the gas in the protogalaxy is likely to be heated and driven away from the BH, once again resulting in sub-Eddington accretion rates (Pelupey et al. 2007).

We have also calculated the number of He II-ionizing photons emitted by the accreting BH, and find that this is within a factor of $\lesssim 2$ of the number of hydrogen-ionizing photons, owing to the high temperatures of the accretion disk. Thus, if Pop III relic BHs are able to accrete efficiently, they may also contribute to the reionization of helium, driving He III regions that can be as large as their H II regions (Furlanetto & Oh 2007).

7 SUMMARY AND CONCLUSIONS

We have investigated the formation of the first galaxies with highly resolved numerical simulations, taking into account all relevant primordial chemistry and cooling. The first galaxies form at redshifts $z \gtrsim 10$ and are characterized by the onset of atomic hydrogen cooling, once the virial temperature exceeds $\simeq 10^4$ K, and their ability to retain photoheated gas. We have described the merger history of a $\simeq 5 \times 10^7 M_{\odot}$ system in great detail and found that in the absence of stellar feedback 10 Pop III.1 stars form

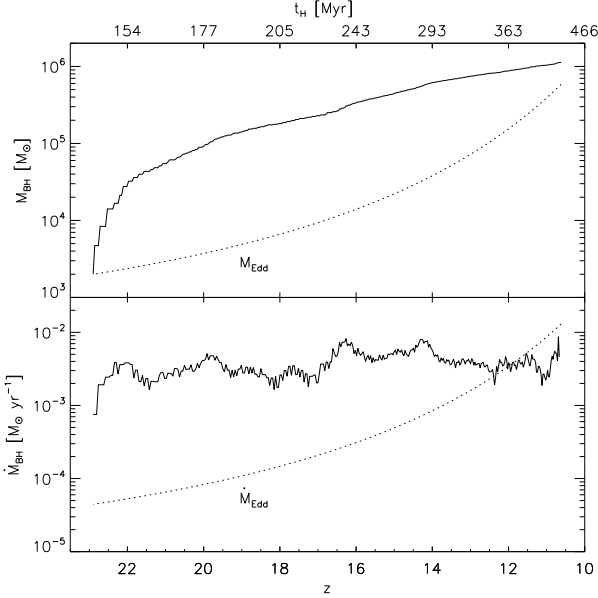


Figure 13. The mass (top panel) and accretion rate (bottom panel) of the central BH as a function of redshift, shown for the simulation (solid lines) and Eddington-limited accretion (dotted lines). The accretion rate remains roughly constant at $\simeq 5 \times 10^{-3} M_{\odot} \text{ yr}^{-1}$, such that the BH grows from $\simeq 2 \times 10^3$ to $\simeq 10^6 M_{\odot}$ in the course of $\simeq 300$ Myr. This is a strict upper limit as radiation effects are not taken into account. Accretion is initially super-Eddington due to the high amount of cold gas brought to the center of the galaxy, but stagnates once turbulence becomes important and the fraction of unbound gas increases.

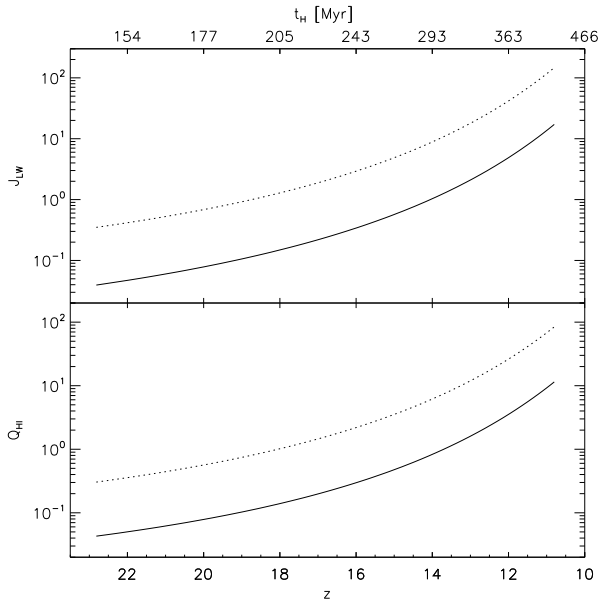


Figure 14. The radiation due to thermal emission from the accretion disk surrounding a Pop III relic BH accreting at the Eddington limit, for an initial mass of 100 (solid lines) and 500 M_{\odot} (dotted lines). *Top panel:* The photodissociating flux, J_{LW} , in units of $10^{-21} \text{ erg s}^{-1} \text{ cm}^{-2} \text{ Hz}^{-1} \text{ sr}^{-1}$, at a distance of 1 kpc from the BH. *Bottom panel:* The number of hydrogen-ionizing photons emitted per second from the accretion disk, in units of 10^{50} s^{-1} .

in minihaloes prior to the assembly of the galaxy. Infalling gas is partially ionized at the virial shock and forms a high amount of H_2 and HD, allowing the gas to cool to the temperature of the CMB and likely form Pop III.2 stars with $\gtrsim 10 M_{\odot}$. Accretion onto the galaxy proceeds initially via hot accretion, where gas is accreted directly from the IGM and shock-heated to the virial temperature, but is quickly accompanied by a phase of cold accretion, where the gas cools in filaments before flowing into the parent halo with high velocities. The latter drives supersonic turbulence at the center of the galaxy and thus plays a key role for second-generation star formation. Finally, we have investigated the growth of BHs seeded by the stellar remnants of Pop III.1 stars and found that accretion at the Eddington limit might be possible under the most favourable circumstances, but in most cases radiation emitted by the progenitor star and the accretion disk around the BH will lead to sub-Eddington accretion rates.

Depending on the strength of radiative and SN-driven feedback, some galaxies might remain metal-free and form intermediate-mass Pop III.2 stars. The inclusion of radiative feedback would likely increase the fraction of Pop III.2 material, as it enhances the degree of ionization, and, consequently, the amount of molecules formed (Johnson et al. 2007a; Wise & Abel 2007c). Observational signatures of intermediate-mass primordial stars might include gamma-ray bursts (GRBs) for the case of a rapidly rotating progenitor (e.g. Bromm & Loeb 2006), or distinct abundance patterns produced by core-collapse SNe experiencing fallback (Umeda & Nomoto 2003). However, since the number of Pop III.1 stars formed in minihaloes prior to the assembly of the galaxy is of order 10, it seems much more likely that at least one star will end in a violent SN explosion and pre-enrich the halo to supercritical levels (Bromm et al. 2003; Greif et al. 2007; Wise & Abel 2007c). In combination with the onset of turbulence, metal mixing in the first galaxies will likely be highly efficient and could lead to the formation of the first low-mass star clusters (Clark et al. 2008), in extreme cases possibly even to metal-poor globular clusters (Bromm & Clarke 2002). Some of the extremely iron-deficient, but carbon and oxygen-enhanced stars observed in the halo of the Milky Way may thus have formed as early as redshift $z \simeq 10$.

In future work, we plan to include the effects of radiative and SN-driven feedback by previous star formation in minihaloes, as well as the distribution of metals and its concomitant cooling. We will study the fragmentation of gas accumulating at the center of the galaxy and address the issue of turbulence-driven star formation in detail. The goal of making realistic predictions for the first generation of starburst-galaxies, to be observed with the *James Webb Space Telescope (JWST)*, is clearly coming within reach.

ACKNOWLEDGMENTS

T.G. would like to thank Chris Burns at the Texas Visualization Laboratory for help with the images presented in this paper. V.B. acknowledges support from NSF grant AST-0708795 and NASA *Swift* grant NNX07AJ636. The simulations presented here were carried out at the Texas Advanced Computing Center (TACC).

REFERENCES

- Abel T., Bryan G. L., Norman M. L., 2000, *ApJ*, 540, 39
- Abel T., Bryan G. L., Norman M. L., 2002, *Sci*, 295, 93
- Abel T., Wise J. H., Bryan G. L., 2007, *ApJ*, 659, L87
- Ahn K., Shapiro P. R., 2007, *MNRAS*, 375, 881
- Alvarez M. A., Bromm V., Shapiro P. R., 2006, *ApJ*, 639, 621
- Ballesteros-Paredes J., Klessen R. S., Mac Low M.-M., Vazquez-Semadeni E., 2007, in Reipurth B., Jewitt D., Keil K., eds, *Protostars and Planets V Molecular Cloud Turbulence and Star Formation*. pp 63–80
- Barkana R., Loeb A., 2001, *Phys. Rep.*, 349, 125
- Beers T. C., Christlieb N., 2005, *ARA&A*, 43, 531
- Begelman M. C., Volonteri M., Rees M. J., 2006, *MNRAS*, 370, 289
- Bromm V., Clarke C. J., 2002, *ApJ*, 566, L1
- Bromm V., Coppi P. S., Larson R. B., 1999, *ApJ*, 527, L5
- Bromm V., Coppi P. S., Larson R. B., 2002, *ApJ*, 564, 23
- Bromm V., Ferrara A., Coppi P. S., Larson R. B., 2001, *MNRAS*, 328, 969
- Bromm V., Kudritzki R. P., Loeb A., 2001, *ApJ*, 552, 464
- Bromm V., Larson R. B., 2004, *ARA&A*, 42, 79
- Bromm V., Loeb A., 2003a, *ApJ*, 596, 34
- Bromm V., Loeb A., 2003b, *Nat*, 425, 812
- Bromm V., Loeb A., 2004, *New Astron.*, 9, 353
- Bromm V., Loeb A., 2006, *ApJ*, 642, 382
- Bromm V., Yoshida N., Hernquist L., 2003, *ApJ*, 596, L135
- Cen R., Riquelme M. A., 2008, *ApJ*, 674, 644
- Choudhury T. R., Ferrara A., Gallerani S., 2008, *MNRAS*, pp L15+
- Christlieb N., Bessell M. S., Beers T. C., Gustafsson B., Korn A., Barklem P. S., Karlsson T., Mizuno-Wiedner M., Rossi S., 2002, *Nat*, 419, 904
- Ciardi B., Ferrara A., 2005, *Space Sci. Rev.*, 116, 625
- Clark P. C., Glover S. C. O., Klessen R. S., 2008, *ApJ*, 672, 757
- Dijkstra M., Haiman Z., Rees M. J., Weinberg D. H., 2004, *ApJ*, 601, 666
- Eisenstein D. J., Hut P., 1998, *ApJ*, 498, 137
- Frebel A., et al., 2005, *Nat*, 434, 871
- Frebel A., Johnson J. L., Bromm V., 2007, *MNRAS*, 380, L40
- Furlanetto S., Oh S. P., 2007, *ApJ*, submitted (arXiv:0711.1542)
- Gao L., White S. D. M., Jenkins A., Frenk C. S., Springel V., 2005, *MNRAS*, 363, 379
- Gao L., Yoshida N., Abel T., Frenk C. S., Jenkins A., Springel V., 2007, *MNRAS*, 378, 449
- Glover S., 2005, *Space Sci. Rev.*, 117, 445
- Glover S. C. O., Brand P. W. J. L., 2001, *MNRAS*, 321, 385
- Greif T. H., Bromm V., 2006, *MNRAS*, 373, 128
- Greif T. H., Johnson J. L., Bromm V., Klessen R. S., 2007, *ApJ*, 670, 1
- Haiman Z., Bryan G. L., 2006, *ApJ*, 650, 7
- Heger A., Fryer C. L., Woosley S. E., Langer N., Hartmann D. H., 2003, *ApJ*, 591, 288
- Heger A., Woosley S. E., 2002, *ApJ*, 567, 532
- Heitmann K., Lukić Z., Habib S., Ricker P. M., 2006, *ApJ*, 642, L85
- Islam R. R., Taylor J. E., Silk J., 2003, *MNRAS*, 340, 647
- Jang-Condell H., Hernquist L., 2001, *ApJ*, 548, 68
- Jappsen A.-K., Glover S. C. O., Klessen R. S., Mac Low M.-M., 2007, *ApJ*, 660, 1332
- Johnson J. L., Bromm V., 2006, *MNRAS*, 366, 247
- Johnson J. L., Bromm V., 2007, *MNRAS*, 374, 1557
- Johnson J. L., Greif T. H., Bromm V., 2007a, *ApJ*, 665, 85
- Johnson J. L., Greif T. H., Bromm V., 2007b, *MNRAS*, submitted (arXiv:0711.4622)
- Karlsson T., Johnson J. L., Bromm V., 2007, *ApJ*, in press (arXiv:0709.4025)
- Kereš D., Katz N., Weinberg D. H., Davé R., 2005, *MNRAS*, 363, 2
- Kitayama T., Yoshida N., 2005, *ApJ*, 630, 675
- Kitayama T., Yoshida N., Susa H., Umemura M., 2004, *ApJ*, 613, 631
- Klessen R. S., Heitsch F., Mac Low M.-M., 2000, *ApJ*, 535, 887
- Koushiappas S. M., Bullock J. S., Dekel A., 2004, *MNRAS*, 354, 292
- Krumholz M. R., McKee C. F., 2005, *ApJ*, 630, 250
- Kuhlen M., Madau P., 2005, *MNRAS*, 363, 1069
- Larson R. B., 2003, *Rep. Prog. Phys.*, 66, 1651
- Li Y., et al., 2007, *ApJ*, 665, 187
- Lodato G., Natarajan P., 2006, *MNRAS*, 371, 1813
- Lucatello S., Tsangarides S., Beers T. C., Carretta E., Gratton R. G., Ryan S. G., 2005, *ApJ*, 625, 825
- Mac Low M.-M., Ferrara A., 1999, *ApJ*, 513, 142
- Mac Low M.-M., Klessen R. S., 2004, *Rev. Mod. Phys.*, 76, 125
- Machacek M. E., Bryan G. L., Abel T., 2001, *ApJ*, 548, 509
- Machida M. N., Tomisaka K., Nakamura F., Fujimoto M. Y., 2005, *ApJ*, 622, 39
- Mackey J., Bromm V., Hernquist L., 2003, *ApJ*, 586, 1
- Madau P., Ferrara A., Rees M. J., 2001, *ApJ*, 555, 92
- Madau P., Quataert E., 2004, *ApJ*, 606, L17
- Madau P., Rees M. J., 2001, *ApJ*, 551, L27
- Makishima K., Kubota A., Mizuno T., Ohnishi T., Tashiro M., Aruga Y., Asai K., Dotani T., Mitsuda K., Ueda Y., Uno S., Yamaoka K., Ebisawa K., Kohmura Y., Okada K., 2000, *ApJ*, 535, 632
- McGreer I. D., Bryan G. L., 2008, *ApJ*, submitted (arXiv:0802.3918)
- McKee C. F., Tan J. C., 2007, *ApJ*, submitted (arXiv:0711.1377)
- Mesinger A., Bryan G. L., Haiman Z., 2006, *ApJ*, 648, 835
- Mori M., Ferrara A., Madau P., 2002, *ApJ*, 571, 40
- Nagakura T., Omukai K., 2005, *MNRAS*, 364, 1378
- Nakamura F., Umemura M., 2001, *ApJ*, 548, 19
- Navarro J. F., White S. D. M., 1994, *MNRAS*, 267, 401
- Norman M. L., O'Shea B. W., Paschos P., 2004, *ApJ*, 601, L115
- Oh S. P., Haiman Z., 2002, *ApJ*, 569, 558
- Omukai K., Palla F., 2003, *ApJ*, 589, 677
- Omukai K., Tsuribe T., Schneider R., Ferrara A., 2005, *ApJ*, 626, 627
- Omukai K., Yoshii Y., 2003, *ApJ*, 599, 746
- O'Shea B. W., Norman M. L., 2007, *ApJ*, 654, 66
- O'Shea B. W., Norman M. L., 2008, *ApJ*, 673, 14
- Pelupessy F. I., Di Matteo T., Ciardi B., 2007, *ApJ*, 665, 107
- Press W. H., Schechter P., 1974, *ApJ*, 187, 425

- Pringle J. E., 1981, *ARA&A*, 19, 137
- Read J. I., Pontzen A. P., Viel M., 2006, *MNRAS*, 371, 885
- Reed D. S., Bower R., Frenk C. S., Jenkins A., Theuns T., 2007, *MNRAS*, 374, 2
- Rees M. J., 1984, *ARA&A*, 22, 471
- Ricotti M., Gnedin N. Y., Shull J. M., 2001, *ApJ*, 560, 580
- Ricotti M., Gnedin N. Y., Shull J. M., 2002a, *ApJ*, 575, 33
- Ricotti M., Gnedin N. Y., Shull J. M., 2002b, *ApJ*, 575, 49
- Ricotti M., Gnedin N. Y., Shull J. M., 2008, *ApJ*, submitted (arXiv:0802.2715)
- Ricotti M., Ostriker J. P., 2004, *MNRAS*, 350, 539
- Ripamonti E., 2007, *MNRAS*, 376, 709
- Salvaterra R., Ferrara A., Schneider R., 2004, *New Astron.*, 10, 113
- Sancisi R., Fraternali F., Oosterloo T., van der Hulst J. M., 2008, *A&AR*, submitted (arXiv:0803.0109)
- Santoro F., Shull J. M., 2006, *ApJ*, 643, 26
- Scannapieco E., Ferrara A., Madau P., 2002, *ApJ*, 574, 590
- Schaerer D., 2002, *A&A*, 382, 28
- Schneider R., Ferrara A., Natarajan P., Omukai K., 2002, *ApJ*, 571, 30
- Schneider R., Ferrara A., Salvaterra R., Omukai K., Bromm V., 2003, *Nat*, 422, 869
- Schneider R., Omukai K., Inoue A. K., Ferrara A., 2006, *MNRAS*, 369, 1437
- Sheth R. K., Tormen G., 2002, *MNRAS*, 329, 61
- Smith B. D., Sigurdsson S., 2007, *ApJ*, 661, L5
- Spaans M., Silk J., 2006, *ApJ*, 652, 902
- Spergel D. N., Verde L., Peiris H. V., Komatsu E., Nolte M. R., Bennett C. L., Halpern M., Hinshaw G., Jarosik N., Kogut A., Limon M., Meyer S. S., Page L., Tucker G. S., Weiland J. L., Wollack E., Wright E. L., 2003, *ApJS*, 148, 175
- Susa H., Umemura M., 2006, *ApJ*, 645, L93
- Tan J. C., McKee C. F., 2004, *ApJ*, 603, 383
- Tan J. C., McKee C. F., 2007, *First Stars III*. AIP Conference Proceedings, submitted (arXiv:0711.4116)
- Thacker R. J., Scannapieco E., Davis M., 2002, *ApJ*, 581, 836
- Thoul A. A., Weinberg D. H., 1996, *ApJ*, 465, 608
- Tormen G., Bouchet F. R., White S. D. M., 1997, *MNRAS*, 286, 865
- Tsuribe T., Omukai K., 2006, *ApJ*, 642, L61
- Tumlinson J., Shull J. M., 2000, *ApJ*, 528, L65
- Tumlinson J., Shull J. M., Venkatesan A., 2003, *ApJ*, 584, 608
- Uehara H., Inutsuka S.-i., 2000, *ApJ*, 531, L91
- Umeda H., Nomoto K., 2003, *Nat*, 422, 871
- Vázquez-Semadeni E., Ballesteros-Paredes J., Klessen R. S., 2003, *ApJ*, 585, L131
- Vierdayanti K., Watarai K.-y., Mineshige S., 2007, *PASJ*, submitted (arXiv:0712.1857)
- Volonteri M., Haardt F., Madau P., 2003, *ApJ*, 582, 559
- Volonteri M., Rees M. J., 2005, *ApJ*, 633, 624
- Volonteri M., Rees M. J., 2006, *ApJ*, 650, 669
- Wada K., Venkatesan A., 2003, *ApJ*, 591, 38
- Whalen D., Abel T., Norman M. L., 2004, *ApJ*, 610, 14
- Whalen D., O'Shea B. W., Smidt J., Norman M. L., 2007, *ApJ*, in press (arXiv:0708.1603)
- Whalen D., van Veelen B., O'Shea B. W., Norman M. L., 2008, *ApJ*, submitted, (arXiv:0801.3698)
- Wise J. H., Abel T., 2007a, *ApJ*, submitted (arXiv:0710.4328)
- Wise J. H., Abel T., 2007b, *ApJ*, 665, 899
- Wise J. H., Abel T., 2007c, *ApJ*, submitted (arXiv:0710.3160)
- Wise J. H., Abel T., 2007d, *ApJ*, 671, 1559
- Wise J. H., Turk M. J., Abel T., 2007, *ApJ*, submitted (arXiv:0710.1678)
- Yoshida N., 2006, *New Astronomy Review*, 50, 19
- Yoshida N., Abel T., Hernquist L., Sugiyama N., 2003, *ApJ*, 592, 645
- Yoshida N., Bromm V., Hernquist L., 2004, *ApJ*, 605, 579
- Yoshida N., Oh S. P., Kitayama T., Hernquist L., 2007, *ApJ*, 663, 687
- Yoshida N., Omukai K., Hernquist L., 2007, *ApJ*, 667, L117
- Yoshida N., Omukai K., Hernquist L., Abel T., 2006, *ApJ*, 652, 6
- Yoshida N., Sokasian A., Hernquist L., Springel V., 2003, *ApJ*, 598, 73